Magmatic architecture of the Esker intrusive complex in the Ring of Fire intrusive suite, McFaulds Lake greenstone belt, Superior Province, Ontario: Implications for the genesis of Cr and Ni-Cu-(PGE) mineralization in an inflationary dyke-chonolith-sill complex

Michel G. Houlé[1,*], C. Michael Lesher[2], Riku T. Metsaranta[3], Anne-Aurélie Sappin[1], Heather J.E. Carson[2], Ernst M. Schetselaar[4], Vicki McNicoll[4], and Alexandra Laudadio[5]

[1]Geological Survey of Canada, 490 rue de la Couronne, Québec, Quebec G1K 9A9
[2]Department of Earth Sciences, Mineral Exploration Research Centre, Goodman School of Mines, Laurentian University, 935 Ramsey Lake Road, Sudbury, Ontario P3E 2C6
[3]Ontario Geological Survey, 933 Ramsey Lake Road, Sudbury, Ontario P3E 6B5
[4]Geological Survey of Canada, 601 Booth Street, Ottawa, Ontario K1A 0E8
[5]Carleton University, Department of Earth Sciences, 1125 Colonel By Drive, Ottawa, Ontario K1S 5B6
[*]Corresponding author's e-mail: michel.houle@canada.ca

ABSTRACT

One of the dominant geological features in the arcuate, >175 km long, Mesoarchean to Neoarchean McFaulds Lake greenstone belt in northern Ontario is the semi-continuous trend of mafic to ultramafic intrusions belonging to the Ring of Fire intrusive suite, which hosts world-class Cr mineralization, major Ni-Cu-(PGE) mineralization, and potentially significant Fe-Ti-V-(P) mineralization. It appears to have been emplaced over a relatively short time interval of approximately 4 to 4.5 million years. The intrusive suite contains two subsuites: the less widely distributed Koper Lake subsuite, which consists of komatiitic ultramafic-dominated intrusions and typically hosts Cr and Ni-Cu-(PGE) mineralization (e.g. Esker intrusive complex), and the more widely distributed Ekwan River subsuite, which consists of tholeiitic high-Fe-Ti mafic-dominated intrusions and typically hosts Fe-Ti-V-(P) mineralization (e.g. Thunderbird intrusion).

The Esker intrusive complex contains the majority of the known Cr and Ni-Cu-(PGE) mineralization in the Ring of Fire intrusive suite. It is a semi-continuous, structurally rotated, subvertical ultramafic-mafic sill-like body that is composed of multiple intrusions with morphologies that vary from bladed dyke morphologies (e.g. Eagle's Nest), transitional dyke/chonolith morphologies (e.g. Double Eagle, AT-3, and AT-8), to some with transitional chonolith/sill morphologies (e.g. Black Thor). It extends over more than 16 km, youngs to the south-southeast, and is bordered to the north-northwest by several keel-like ultramafic intrusive bodies (e.g. AT-12, C-6, AT-5, AT-1). Clear connections between AT-12 and AT-1 and the overlying Black Thor and Double Eagle intrusions, respectively, and the continuous spectrum of intrusion morphologies suggest that the keels were originally subhorizontal blade-shaped dykes (e.g. Eagle's Nest), the upper parts of which expanded laterally to form transitional dykes/chonoliths (e.g. Double Eagle intrusion) and chonoliths/sills (e.g. Black Thor intrusion), which inflated laterally and coalesced over time to form the sill-like Esker intrusive complex.

Most of the Ni-Cu-(PGE) mineralization in the Esker intrusive complex appears to have formed by incorporation of sulphur from footwall oxide-silicate-sulphide iron formations, a process that is similar to most other komatiite-associated Ni-Cu-(PGE) deposits worldwide. A fundamental issue in the genesis of all stratiform chromite deposits is how to form thick layers of massive to semi-massive chromite, an issue exacerbated by the vast amounts of chromite in the Esker intrusive complex. A genetic model that resolves the mass balance problem involves partial melting of Fe±Ti oxide-rich rocks (oxide-facies iron formation or ferrogabbro) and conversion of fine-grained oxide xenocrysts to chromite by reaction with Cr-rich komatiitic magma in a dynamic magma conduit. This model has been recently challenged based on the capacity of komatiitic magma to dissolve large amounts of magnetite, which would prevent upgrading. However, alternative models cannot explain the presence of composite chromite-silicate-sulphide grains with textures like

Houlé, M.G., Lesher, C.M., Metsaranta, R.T., Sappin, A.-A., Carson, H.J.E., Schetselaar, E.M., McNicoll, V., and Laudadio, A., 2020. Magmatic architecture of the Esker intrusive complex in the Ring of Fire intrusive suite, McFaulds Lake greenstone belt, Superior Province, Ontario: Implications for the genesis of Cr and Ni-Cu-(PGE) mineralization in an inflationary dyke-chonolith-sill complex; *in* Targeted Geoscience Initiative 5: Advances in the understanding of Canadian Ni-Cu-PGE and Cr ore systems – Examples from the Midcontinent Rift, the Circum-Superior Belt, the Archean Superior Province, and Cordilleran Alaskan-type intrusions, (ed.) W. Bleeker and M.G. Houlé; Geological Survey of Canada, Open File 8722, p. 141–163. https://doi.org/10.4095/326892

those in footwall magnetite-silicate-sulphide facies iron formations. More research is required to reconcile the discrepancies.

Regardless of their origin, the wide diversity of mineral deposit types in the McFaulds Lake greenstone belt, including world-class Cr, significant Ni-Cu-(PGE), and potential Fe-Ti-V-(P) mineralization related to mafic and ultramafic rocks, make the Ring of Fire region an excellent exploration target to increase the world's supply of critical minerals.

INTRODUCTION

The Mesoarchean to Neoarchean McFaulds Lake greenstone belt (a.k.a. Ring of Fire region; Metsaranta and Houlé, 2020) in northern Ontario is recognized as one of the next emerging major mineral districts in Canada, containing world-class magmatic Cr deposits, a major Ni-Cu-(PGE) deposit and numerous occurrences, small volcanogenic massive Cu-Zn sulphide deposits, significant Fe-Ti-V-(P) prospects, and several kimberlitic diamond and orogenic Au occurrences (*see* Metsaranta and Houlé, 2020).

Over the past decade, the Geological Survey of Canada (GSC) and the Ontario Geological Survey (OGS), in collaboration with numerous exploration companies and academic collaborators, have undertaken a diverse range of geoscience activities in the Ring of Fire region. This research has significantly increased our knowledge of the Cr, Ni-Cu-(PGE) and Fe-Ti-V-(P) mineralized ultramafic to mafic intrusions and their overall geological context (Metsaranta and Houlé, 2020 and references therein).

In this contribution, we summarize the main characteristics of the McFaulds Lake greenstone belt, the Ring of Fire intrusive suite, and their associated orthomagmatic Cr, Ni-Cu-(PGE), and Fe-Ti-V mineralization, and briefly address some key components of the magmatic architecture of this well endowed ultramafic to mafic ore system in northern Ontario.

McFAULDS LAKE GREENSTONE BELT

The geology of the Ring of Fire region, located in the central part of the northern Superior Province, comprises a variety of Precambrian supracrustal and intrusive rocks, flat-lying Paleozoic cover rocks, and Quaternary deposits. The poorly exposed Precambrian geology includes Mesoarchean to Neoarchean supracrustal rocks of the McFaulds Lake greenstone belt and a variety of felsic to ultramafic intrusive rocks (Fig. 1), as well as Proterozoic dyke swarms (Matachewan, Marathon, Pickle Crow, Mackenzie: Stott and Josey, 2009) and kimberlitic intrusions (Kyle Lake kimberlites: Sage, 2000). The paucity of outcrop was one of the major reasons for the lack of interest in this region from the provincial/federal geological surveys and mineral explorers until the discoveries of the Kyle diamondiferous kimberlites in the mid-1990s. The subsequent discovery of the McFaulds Cu-Zn volcanogenic massive sulphide (VMS)-style mineralization in 2002 led to an increase of exploration efforts in the region and the discovery of the Big Daddy Cr mineralization in 2006 and the Eagle One (now known as Eagle's Nest) Ni-Cu-(PGE) mineralization in 2007 (*see* Exploration History for more details in Metsaranta and Houlé, 2020).

The McFaulds Lake greenstone belt is an arcuate (>175 km long) greenstone belt that records episodic volcanism and sedimentation spanning from ca. 2.83 Ga to 2.70 Ga (e.g. Metsaranta et al., 2015; Metsaranta and Houlé, 2020). It has been subdivided into eight lithotectonic assemblages: two late Mesoarchean to early Neoarchean assemblages comprising volcanic rocks of mostly tholeiitic affinity with lesser amounts of volcanic rocks of komatiitic and calc-alkalic affinities (Butler: ca. 2828 Ma; Attawapiskat: ca. 2820–2797 Ma); two early Neoarchean volcanic-dominated assemblages of tholeiitic and calc-alkalic affinities (Victory: ca. 2783–2780 Ma; Winiskisis: ca. 2757 Ma); three middle Neoarchean assemblages dominated by volcanic rocks of calc-alkalic affinity with minor amounts of volcanic rocks with tholeiitic and komatiitic affinities (Muketei: ca. 2737–2734 Ma; Oval: >2711 Ma; Kitchie: <2725 Ma); and one very poorly exposed sedimentary rock-dominated assemblage (Tappan: <2702 Ma) (Fig. 2; Metsaranta and Houlé, 2020).

One particularity of the McFaulds Lake greenstone belt that was highlighted by recent OGS and GSC work is that almost the entire metal endowment of the Ring of Fire region is closely associated with the 2737–2734 Ma Muketei assemblage and the widespread, coeval mafic to ultramafic magmatism of the Ring of Fire intrusive suite, which includes the well endowed ultramafic to mafic Esker intrusive complex (Fig. 2).

The McFaulds Lake greenstone belt, like most other Archean greenstone belts across the Superior Province, experienced several phases of deformation and metamorphism, up to upper amphibolite facies that affected, to varying degrees, the preservation of this greenstone belt (*see* Metsaranta and Houlé, 2020). In the central part of the McFaulds Lake greenstone belt, metamorphic grades appear to be lower than elsewhere in the belt. The Esker intrusive complex displays well preserved igneous textures, has been metamorphosed to the lower to middle greenschist facies, and is only

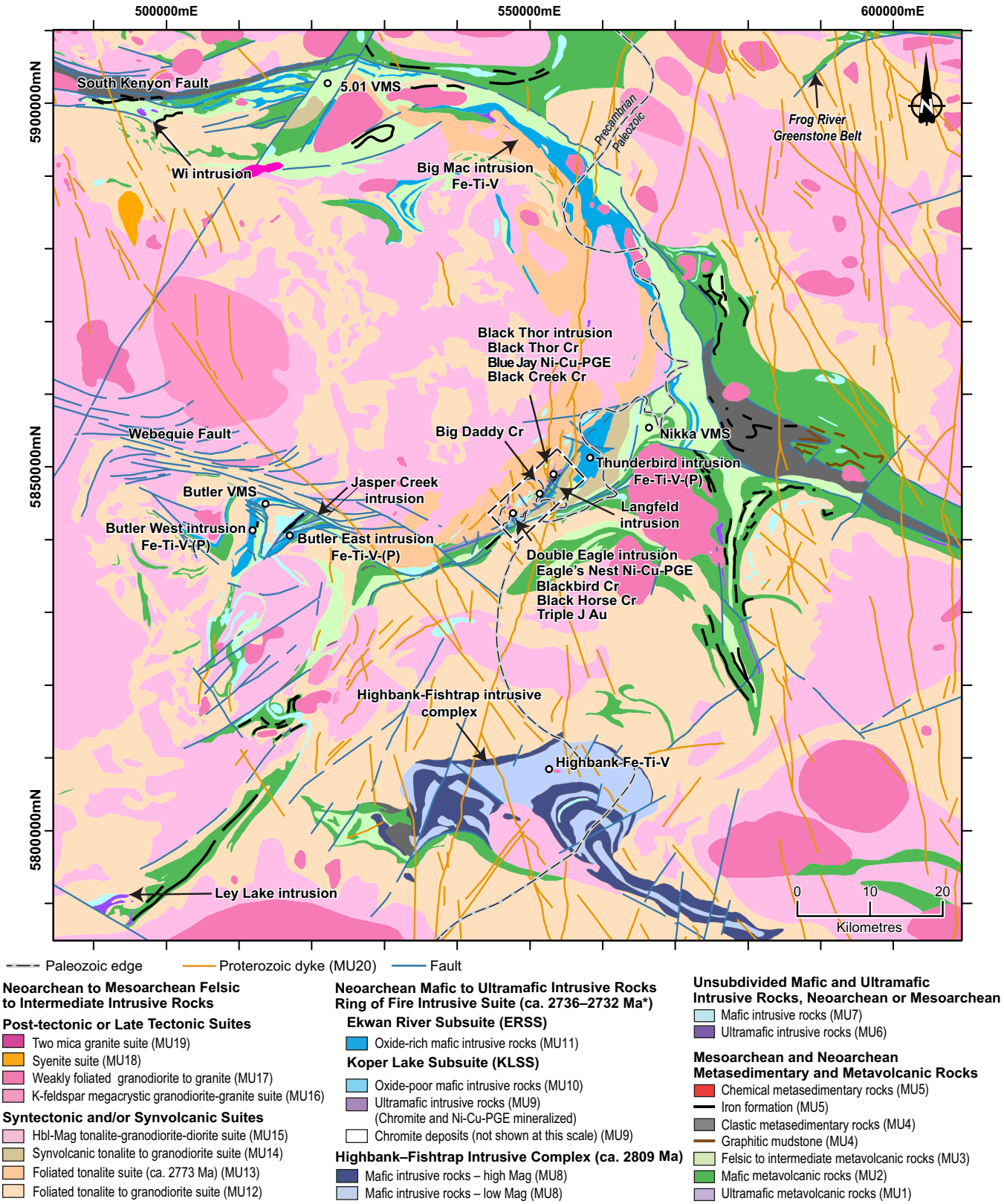

Figure 1. Geological map of the McFaulds Lake and southeast extension of the Frog River greenstone belts showing the location of the main mineral deposits and occurrences in the Ring of Fire region (*modified from* Metsaranta and Houlé, 2017a,b,c). Paleozoic cover rocks occur to the east of the Paleozoic edge line. Trace of the fold axial plane is omitted for clarity. Dashed black box indicates the location of Figure 5. Cooridnates in Universal Transverse Mercator (UTM)–North America Datum 1983 (NAD83)–Zone 16. Abbreviations: Hbl = hornblende, K-feldspar = potassium feldspar, Mag = magnetite, MU = map units used in Metsaranta and Houlé (2017a,b,c, 2020). *The age interval for the Ring of Fire intrusive suite is rounded and takes errors into account.

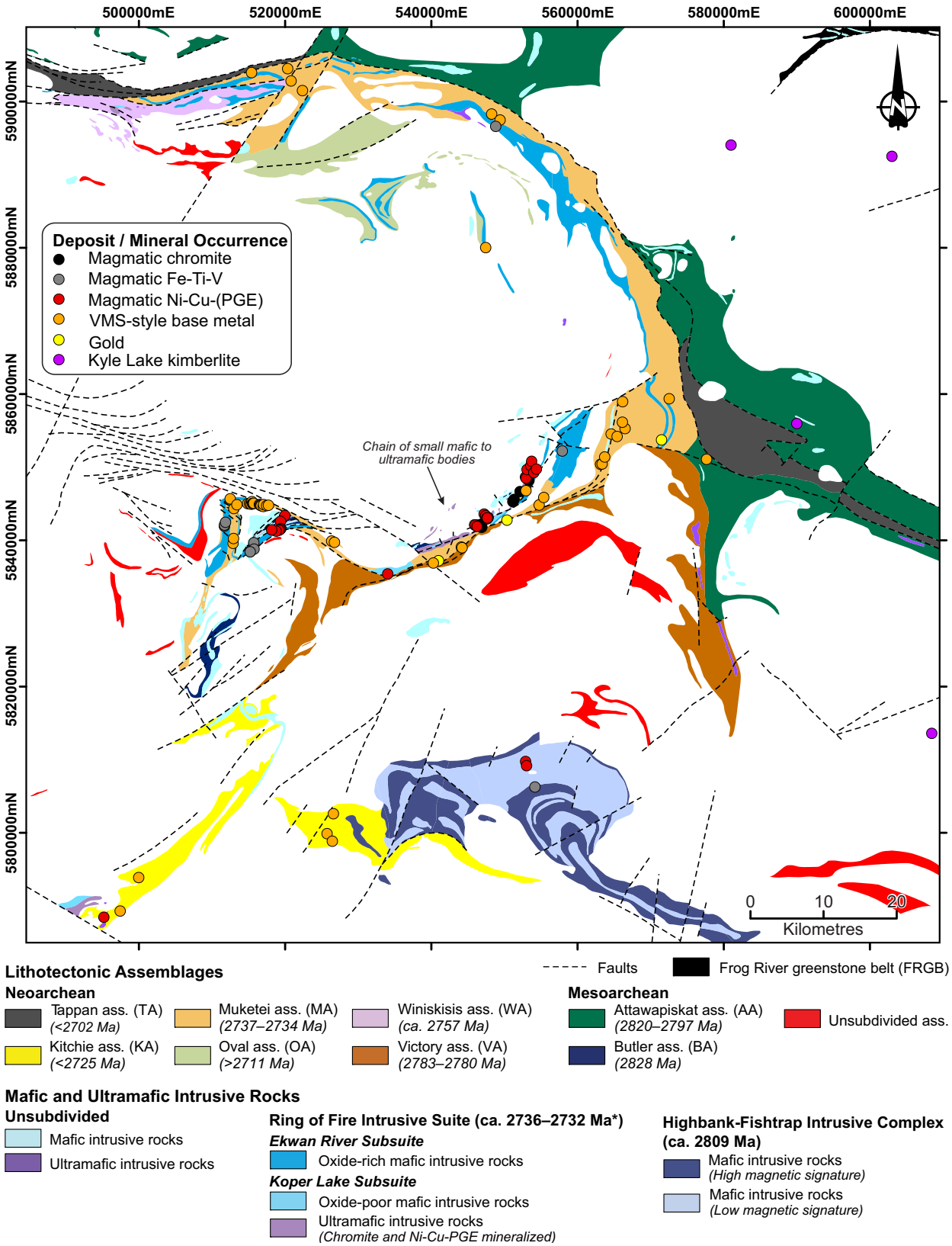

Figure 2. Simplified geological map showing the distribution of the lithotectonic assemblages for supracrustal rocks and the distribution of mafic to ultramafic intrusions in the McFaulds Lake greenstone belt (*modified from* Metsaranta and Houlé, 2020). Coordinates in UTM NAD83, Zone 16. Abbreviations: ass. = assemblage as defined by Metsaranta and Houlé (2020), VMS = volcanogenic massive sulphides. *The age interval for the Ring of Fire intrusive suite is rounded and takes errors into account.

locally deformed, in which most of the rocks do not exhibit any strong penetrative structural fabrics.

Ring of Fire Intrusive Suite

The dominant mafic and ultramafic intrusions in the Ring of Fire region represent a large mafic to ultramafic magmatic event recognized as the Ring of Fire intrusive suite (e.g. Mungall et al., 2011; Houlé et al., 2015; Metsaranta et al., 2015), which were emplaced along the entire strike length of the McFaulds Lake greenstone belt over a relatively short time period of a few million years (*see* Timing and Relationship of Koper Lake and Ekwan River Subsuites; Fig. 2). Two major types of mafic to ultramafic intrusions have been recognized in the McFaulds Lake greenstone belt (e.g. Metsaranta et al., 2015; Houlé et al., 2015) and have been subdivided by Houlé et al. (2019) into the Ekwan River and the Koper Lake subsuites based on their spatial distribution, lithological association, geochemical signature, and mineralization styles.

Ekwan River subsuite

The Ekwan River subsuite is dominated by Fe-oxide-bearing mafic rocks and is composed of abundant gabbro, melagabbro, and leucogabbro with lesser anorthosite and rare pyroxenite. This subsuite occurs over the entire length of the McFaulds Lake greenstone belt (Fig. 1, 2). It hosts most of the Fe-Ti-V-(P) mineralization in the region, the best examples being the Thunderbird, Butler West, Butler East (Kuzmich et al., 2015), and Big Mac (Sappin et al., 2015) intrusions, which are relatively continuous over significant strike lengths and exhibit strong geophysical anomalies (OGS–GSC, 2011). Almost all of these intrusions contain significant amounts of fine-grained disseminated and lesser semi-massive to massive Fe-Ti-V oxides (e.g. titanomagnetite, magnetite, ilmenite), whereas only a few contain phosphates (apatite). The mineralization is texturally similar from one intrusion to another and occurs in rocks ranging in composition from melagabbro to anorthosite. The Fe-Ti-V ore horizon in the Thunderbird intrusion generally occurs as a thick (100s of metres) interval of disseminated magnetite-ilmenite with sparse, thin (up to 45 cm thick), semi-massive to massive oxide layers (Kuzmich, 2014). In contrast, Fe-Ti-V ore horizons in the Butler intrusions (i.e. Butler East and West intrusions) generally occur as interlayered semi-massive to massive oxides (up to 24 m thick) and heavily disseminated oxides in gabbroic rocks (Kuzmich, 2014).

Rocks of the Ekwan River subsuite range from Mg-Cr-Ti-poor, Al-rich mesogabbro to Mg-Cr-poor, Al-Ti rich ferrogabbro, consistent with fractionation and accumulation of clinopyroxene-plagioclase-ilmenite (Fig. 3). They include Fe-Ti-V-rich, Mg-poor oxide mineralization (Fig. 3a,b,g,h).

Koper Lake subsuite

The Koper Lake subsuite is dominated by ultramafic rocks and is composed of variably serpentinized and/or talc-carbonate-altered dunite, peridotite, chromitite, pyroxenite, and gabbro. This subsuite is relatively restricted geographically, occurring predominantly in the central part of the McFaulds Lake greenstone belt but locally on its peripheries (e.g. Ley and Wi intrusions; Fig. 1, 2). It hosts most of the orthomagmatic Cr and Ni-Cu-PGE mineralization, the best examples of which occur in the Black Thor (Carson et al., 2015, 2016; Carson, in prep) and Double Eagle intrusions (Azar, 2010), and the Eagle's Nest dyke (Mungall et al., 2010; Zuccarelli et al., 2017, 2018a,b, 2020; Zuccarelli, in prep) of the Esker intrusive complex (Houlé et al., 2019). These styles of mineralization are briefly summarized below (*see* Orthomagmatic Mineralization).

Rocks of the Koper Lake subsuite range from Mg±Cr rich, Al-Ti-poor dunite, peridotite, and pyroxenite that exhibit trends consistent with fractionation and accumulation of olivine±chromite to Mg-Cr-poor, Al-Ti rich mesogabbro that exhibits trends consistent with fractionation of clinopyroxene-plagioclase± ilmenite. They include Cr-Al-Mg-rich, Ti-V-poor chromite mineralization (Fig. 3). Two distinct trends are shown in Figure 3 that are characteristic of the Koper Lake and Ekwan River subsuites. The Koper Lake subsuite generally exhibits higher values of Ni and Cr whereas the Ekwan River subsuite generally exhibits higher values of Ti and V (Fig. 3b,d–h). This clear geochemical distinction can be used to correctly discriminate between the two subsuites.

Timing and relationship of the Koper Lake and Ekwan River subsuites

U-Pb single zircon thermal ionization mass spectrometry (TIMS) dating indicates that the Ring of Fire intrusive suite was emplaced over a period of 4 to 4.5 million years between 2736.3 to 2731.8 Ma[1] (Table 1). The oldest date obtained is from the mafic component of the Big Daddy segment of the Black Thor intrusion at ca. 2735.5 ± 0.8 Ma, whereas the youngest dates are from the Wi intrusion at 2732.9 ± 0.6 Ma and the Croal Lake intrusion at 2732.6 ± 0.8 Ma, belonging to the Koper Lake and Ekwan River subsuites, respectively (Table 1). Attempts to date the ultramafic part of the Black Thor intrusion have thus far not been successful, but a late websterite phase that crosscuts the lower part

[1] This age interval for the emplacement of the Ring of Fire intrusive suite has been estimated from the oldest and youngest ages obtained, including the errors on these ages, making this a maximum time duration for its emplacement.

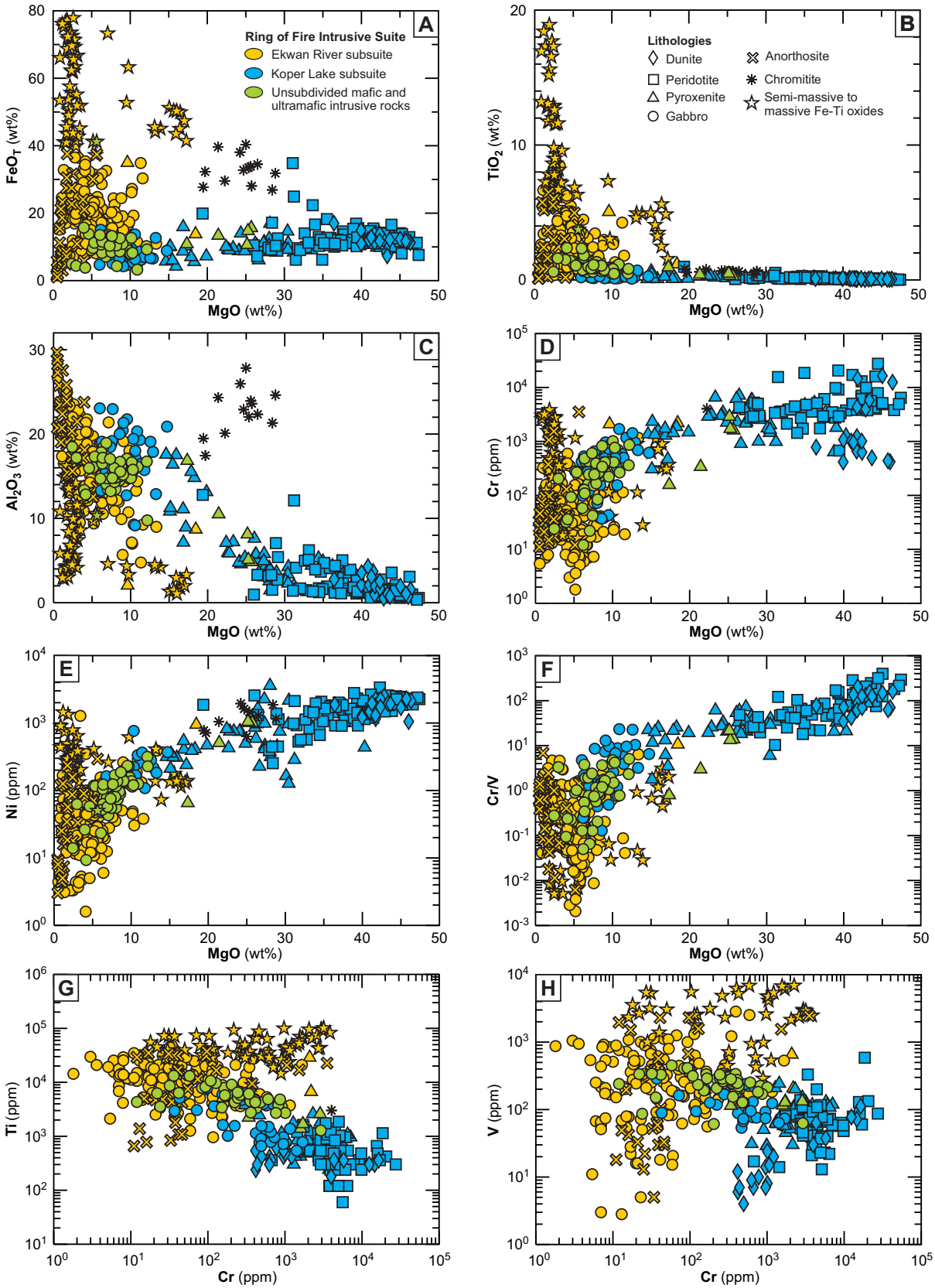

Figure 3. Binary plots of major and trace elements (anhydrous and normalized to 100%) of the mafic to ultramafic intrusions within the Koper Lake and Ekwan River subsuites of the Ring of Fire intrusive suite. **a)** FeO_T versus MgO, **b)** TiO_2 versus MgO, **c)** Al_2O_3 versus MgO, **d)** Cr versus MgO, **e)** Ni versus MgO, **f)** Cr/V versus MgO, **g)** Ti versus Cr, and **h)** V versus Cr. The shape of the symbol indicates the rock types whereas the colour indicates the subsuite to which they belong. Data are *from* Kuzmich et al. (2015), Metsaranta (2017), and Houlé, unpublished data.

Table 1. Lithodemic unit classification scheme as proposed by Houlé et al. (2019) for mafic-ultramafic intrusive rocks in the Ring of Fire intrusive suite with their associated mineralization and age constraints.

Suite	Subsuite	Complex	Lithodeme		U-Pb Age (Ma)	Magmatic Mineralization*
			Intrusion	Segment		
Ring of Fire Intrusive Suite (RoFIS)	Koper Lake Subsuite	Esker Intrusive Complex (EIC)	Black Thor	Black Thor	2734.1±0.6 and 2733.6±0.7	**BT, BL** BJ, BJE, BCZ, NEBZ, CBZ, SWBZ, NOT-08-2G15, NOT-08-2G28
				Black Creek	*Undated*	**BC**
				Big Daddy	2735.5±0.8 and 2733.7±0.8	**BD**
				C-3/C-4	*Undated*	FN-10-21
			C6		*Undated*	–
			AT-5		*Undated*	–
			Double Eagle	AT-1	*Undated*	**BH**, EZ, FN-08-10 FN-08-02, FN-10-01
				Blackbird	*Undated*	**BB1, BB2**, ET
			Eagle's Nest		*Undated*	**EN**
			Wi		2732.9±0.6	–
			Ley Lake		*Undated*	–
			Jasper Creek		*Undated*	–
	Ekwan River Subsuite		Butler West		*No zircon*	BP11-V01/V06/V07
			Butler East		*No zircon*	BP11-V05/V04, MN08-82, McNugget
			Thunderbird		2733.6±0.7	Thunderbird Anomaly
			Big Mac		2734.1±0.8	BM9B-04
			Langfeld		*Undated*	Unamed
			Croal Lake**		2732.6±0.8	Semple-Hulbert
			Pinay		*Pending*	Unamed

*Mineralization text: bold text = deposit, non-bold text = occurrence, black text = Cr-(PGE), red text = Ni-Cu-(PGE), green text = Fe-Ti-V-(P).

**Croal Lake intrusion is not shown on Figure 1. It is located approximately 50 km west-northwest of the northwest corner of the mapping area shown in Figure 1. Geochronology data *from* Houlé et al. (2015a) and this study.

See Figure 5 for abbreviations. NOT-08-2G15 or other combinations are drillhole identifications.

of the intrusion has been dated at 2733.6 ± 0.7 Ma. The textures along the contact between the late websterite phase and the lower part of the Black Thor intrusion suggest that they are more or less coeval (Spath, 2017), suggesting that the Esker intrusive complex was emplaced within an interval of 1.8 to 3.4 million years.

A younger age (2730.5 ± 0.8 Ma) was obtained in the McFaulds Lake greenstone belt for a biotite-bearing gabbro that crosscuts the Black Thor intrusion and it is therefore interpreted to be unrelated to the Ring of Fire intrusive suite (Houlé et al., 2019). Overall, no significant age differences have been observed between intrusions that belong to either the Koper Lake or the Ekwan River subsuites.

Esker intrusive complex

The Esker intrusive complex is a semi-continuous, subvertical ultramafic-mafic body comprising multiple intrusions (e.g. Black Thor, Double Eagle, AT-3, and AT-8) that extends for 16 km from Black Thor intrusion in the northeast to the AT-8 intrusion in the southwest (Fig. 4). The Esker intrusive complex includes several keel-like ultramafic intrusive bodies (e.g. AT-12, C-6, AT-5, AT-1, and Eagle's Nest) to the north-northwest that extend 650–900 m into the granitoid country rocks (Fig. 4). A few distinct magnetic anomalies, which are interpreted to correspond to other ultramafic to mafic intrusive bodies, potentially extend the footprint of the Esker intrusive complex for another 4 km to the southwest.

The base (northwest side) of the Esker intrusive complex is usually in contact with ca. 2773 Ma (e.g. Mungall et al., 2010; Metsaranta et al., 2015; Metsaranta and Houlé, 2020) tonalitic rocks that are locally baked and intruded by the Esker intrusive complex. However, the sparse geological information along the base of the Esker intrusive complex and the presence of thin granitoids within the complex cannot completely discount the possibility that locally younger granitoids may have been intruded along the basal con-

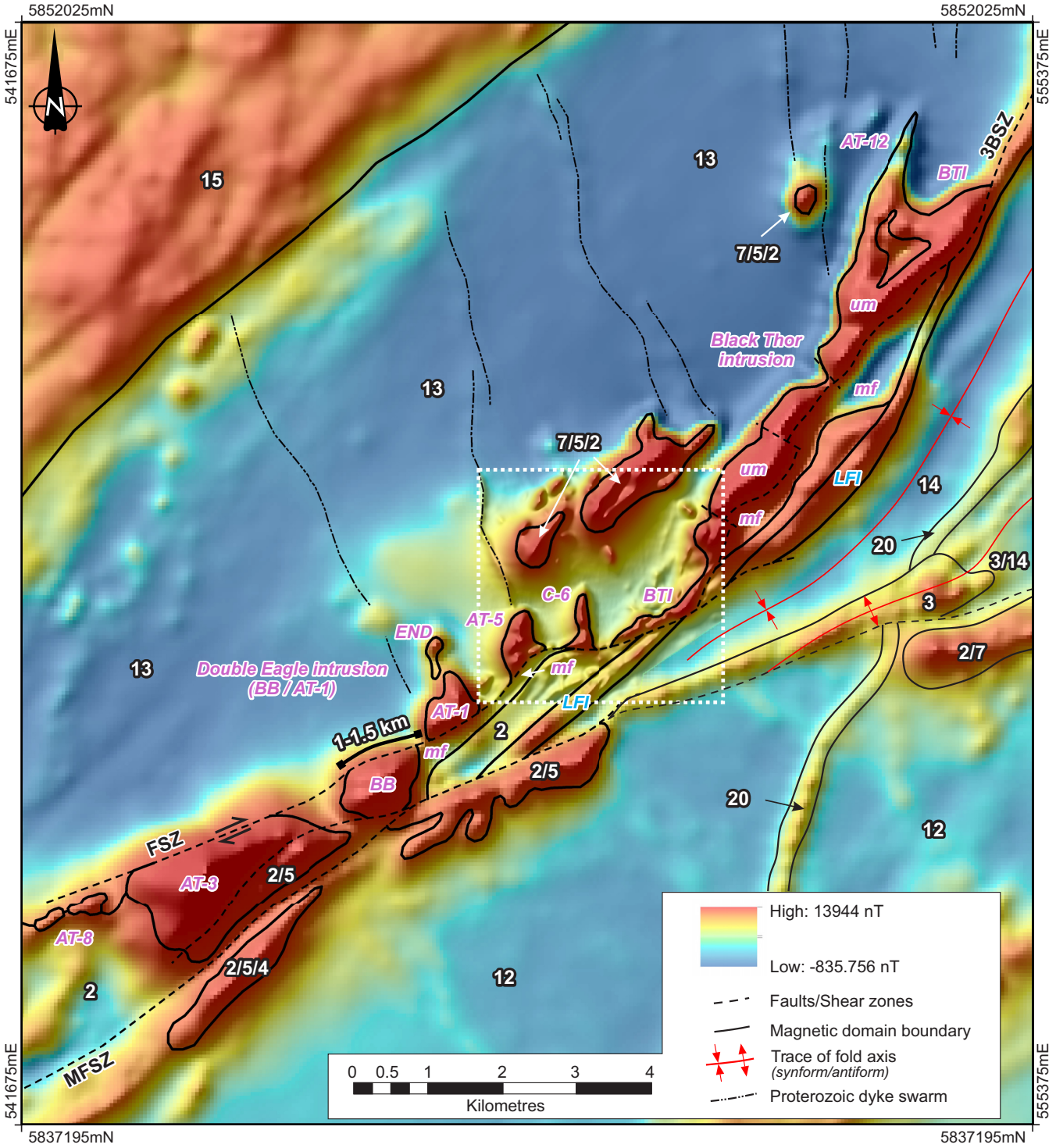

Figure 4. Colour-relief-shaded magnetic data, displayed with histogram equalization, overlain with the revised structural interpretation and magnetic domain boundaries showing the distribution of mafic to ultramafic intrusive bodies of the Esker intrusive complex (*modified from* Laudadio, 2019). White dotted box highlights proprietary high-resolution magnetic data (gridded from 75 m line spacing). Black text labels are faults: FSZ = Frank Shear Zone, MFSZ = McFaulds Lake Shear Zone, 3BSZ = Black Thor-Black Creek-Big Daddy Shear Zone. Purple text labels are part of the Koper Lake subsuite: BTI = Black Thor intrusion, DEI = Double Eagle intrusion, END = Eagle's Nest dyke, mf = mafic component, um = ultramafic component. Blue text labels are part of the Ekwan River subsuite: LFI = Langfeld intrusion. White text labels are map units: 2 = mafic metavolcanic rocks, 3 = felsic to intermediate metavolcanic rocks, 4 = graphitic mudstone, 5 = iron formation and graphitic mudstone, 7 = unsubdivided mafic intrusive rocks, 12 = foliated tonalite to granodiorite suite, 13 = foliated tonalite suite, 14 = synvolcanic tonalite to granodiorite suite, 15 = hornblende-magnetite tonalite-granodiorite-diorite suite, 20 = Proterozoic dyke swarm. Numbers are consistent with the map units in Figure 1.

tact. The tonalitic footwall rocks contain kilometric enclaves of supracrustal rocks, as shown on Figure 5, composed predominantly of mafic intrusive and volcanic rocks within oxide-facies iron formation, which are interpreted to be stratigraphically equivalent of the Butler assemblage by Metsaranta and Houlé (2020). Overall differentiation of the complex from dunitic and peridotitic in the northwest grading to more pyroxenitic to gabbroic in composition to the south-southeast strongly suggest a stratigraphic top in that direction (Fig. 5, 6). In addition, several small ellipsoidal magnetic anomalies trending northeast-southwest in the footwall of the complex (mostly north of AT-8), delineate a chain of mafic to ultramafic intrusions, a few of which have been determined to be peridotitic and ferrogabbroic bodies that most likely belong to the Koper Lake and Ekwan River subsuites, respectively (Fig. 2). Some of these intrusive bodies will be briefly described below, however, the reader is referred to previous (Metsaranta and Houlé, 2020 and references therein) and upcoming publications (Carson, in prep; Farhangi, in prep; Zuccarelli, in prep) from this project for more details about these well mineralized ultramafic to mafic intrusions. Almost all components of the Esker intrusive complex are composed of thick lower olivine-rich ultramafic zones that are normally, but not always, overlain by thinner upper mafic zones.

Black Thor intrusion

The Black Thor intrusion is the largest and the most continuous intrusive body of the Esker intrusive complex. It extends for more than 8 km along strike (Fig. 4, 5) and exhibits the most complete (potentially archetype) section throughout the Koper Lake subsuite. The present surface section (which approximates an original cross-section) consists of a broad trough-shaped sill comprising a thicker ultramafic component overlain by a thinner mafic component (Fig. 5). It appears to have formed by repeated influxes of komatiitic magmas accompanied by crystallization of olivine±orthopyroxene±chromite-rich cumulates and fractionation of the residual liquid (Carson, in prep). The result is a stratigraphy comprising interlayered (from base to top) dunite/harzburgite, harzburgite/websterite/chromitite, and websterite/gabbro (e.g. Tuchscherer et al., 2010; Carson et al., 2015, 2016). The Black Thor intrusive body can be subdivided into three main series: a Basal Series, an Ultramafic Series (with Lower, Middle, and Upper parts), and a Mafic Series, each of which can be further subdivided into several zones (Fig. 6). The reader is referred to Carson (in prep) for a more detailed description of the entire igneous stratigraphy of the Black Thor intrusion. The distribution and the thickness of the series and zones vary across the intrusion, indicating lateral facies variations, with the magma conduit located at the thickest part, at the AT-12 keel in the northeast, with the sequence thinning toward the Big Daddy deposit to the southwest (Fig. 5). The intrusion is cut by the 3B Shear Zone (3BSZ) to the east, but the oblique orientation of the AT-12 keel suggests that magma may have flowed toward the southwest, feeding the more distal (relative to the interpreted conduit) parts of the intrusion. We cannot completely rule out that this geometry could also result from a progressive non-coaxial deformation but it is unlikely based on the facies variations observed in drill cores. The AT-12 keel is ~100–1000 m wide (east-west) and ~1000 m long (north-south) in surface section, narrowing and apparently terminating into the footwall rocks toward the north-northwest (Fig. 5). It contains similar Black Thor Marginal Zone units along the sides grading gradually from pyroxenite at the margins to olivine pyroxenite to peridotite toward the interior. However, the AT-12 keel lithologies have been transgressed by a websterite to a feldspathic websterite (i.e. Late Websterite phase) that extends into the Black Thor intrusion; where it has intruded and brecciated the Lower Ultramafic and Middle Ultramafic Series, including the Black Label Chromite Zone (Spath, 2017). The Late Websterite phase appears to have been emplaced after the Basal Series and Lower Ultramafic Series but before complete solidification, producing a range of hybrid lithologies and incorporating numerous inclusions, including some chromitite inclusions, mainly within its peripheries (Fig. 7a; Spath, 2017). Multiple generations of peridotitic units also occur locally within the Black Thor intrusion, the younger of which contain numerous subrounded to subangular chromitite inclusions and the older of which are completely lacking of any chromitite inclusions or chromitite layers (*see* Fig. 7b). These observations suggest that the chromitite inclusions have been transported from "upstream" in the system. Olivine compositions in this intrusion range between Fo_{94} and Fo_{80} (Laarman, 2014; Spath 2017; Carson, in prep), with the most magnesian analyzed olivine occurring in the Black Label Chromitite Zone.

Double Eagle intrusion

The Double Eagle intrusion is principally composed of two ultramafic bodies (AT-1 and Blackbird) that are dissected by the Frank Shear Zone (Fig. 4, 5). The intrusions appear to correlate based on their magnetic signatures, suggesting 1–1.5 km of dextral displacement (Fig. 4), a correlation supported by 3-D modelling (Laudadio, 2019; also *see* Esker Intrusive Complex Structural Reconstruction). In surface section (which approximates an original cross-section), the restored intrusion has the form of a transitional dyke/chonolith (*see* discussion of morphologies by Barnes and

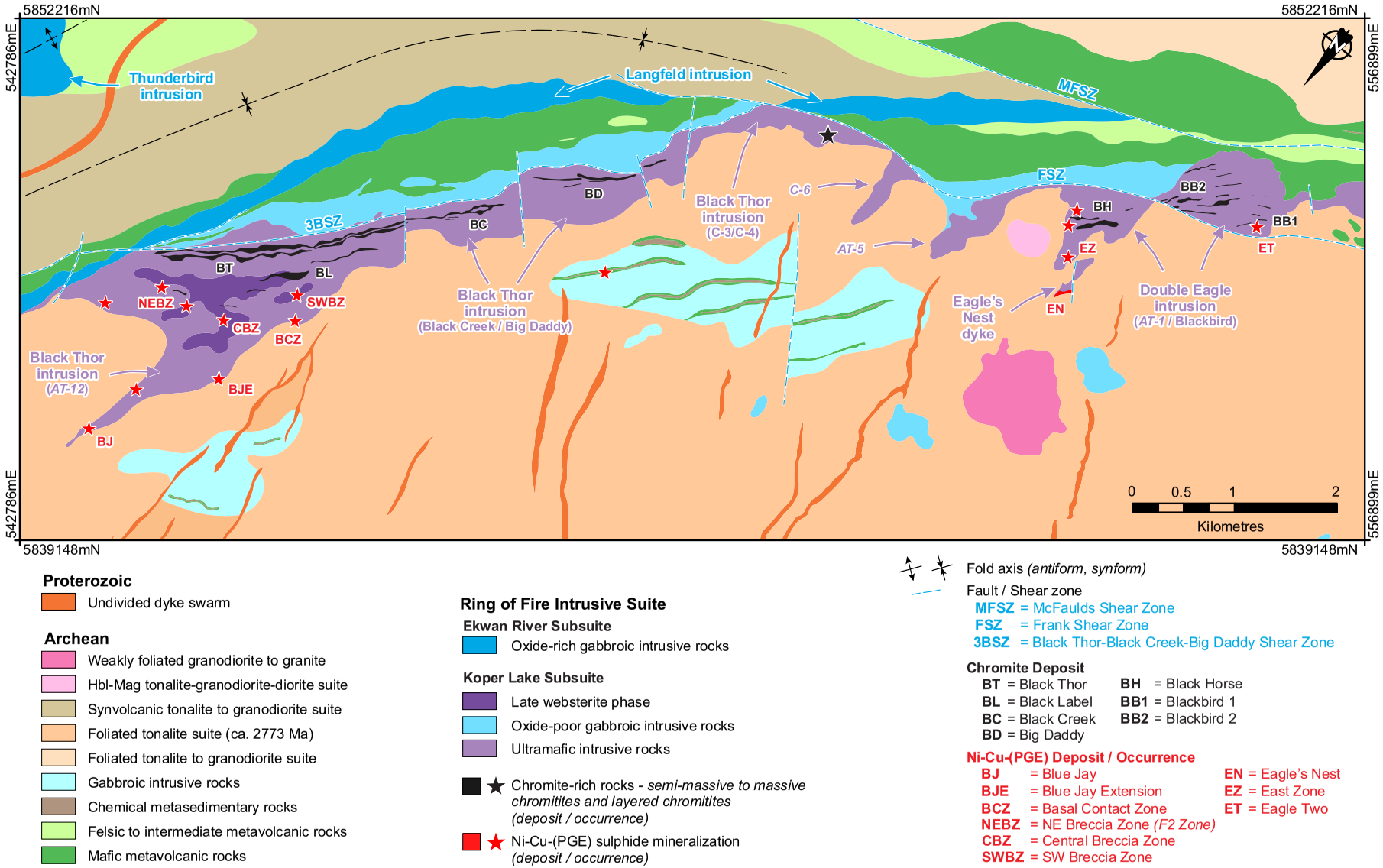

Figure 5. Geological map showing the Esker intrusive complex and associated mineral deposits and occurrences. Geology *adapted from* Metsaranta and Houlé (2017b), Houlé et al. (2017, 2019), Laudadio (2019), and Noront Resources Ltd. (unpub. data). Text in blue = intrusion of the Ekwan River subsuite, purple text = intrusion/keel (*italic*) of the Koper Lake subsuite. Abbreviations: Hbl = hornblende, Mag = magnetite. Chromite and Ni-Cu-(PGE) mineralization shown on the map represent the main mineralized intervals projected to surface. Note that the map has been rotated in order to put the stratigraphic top upward.

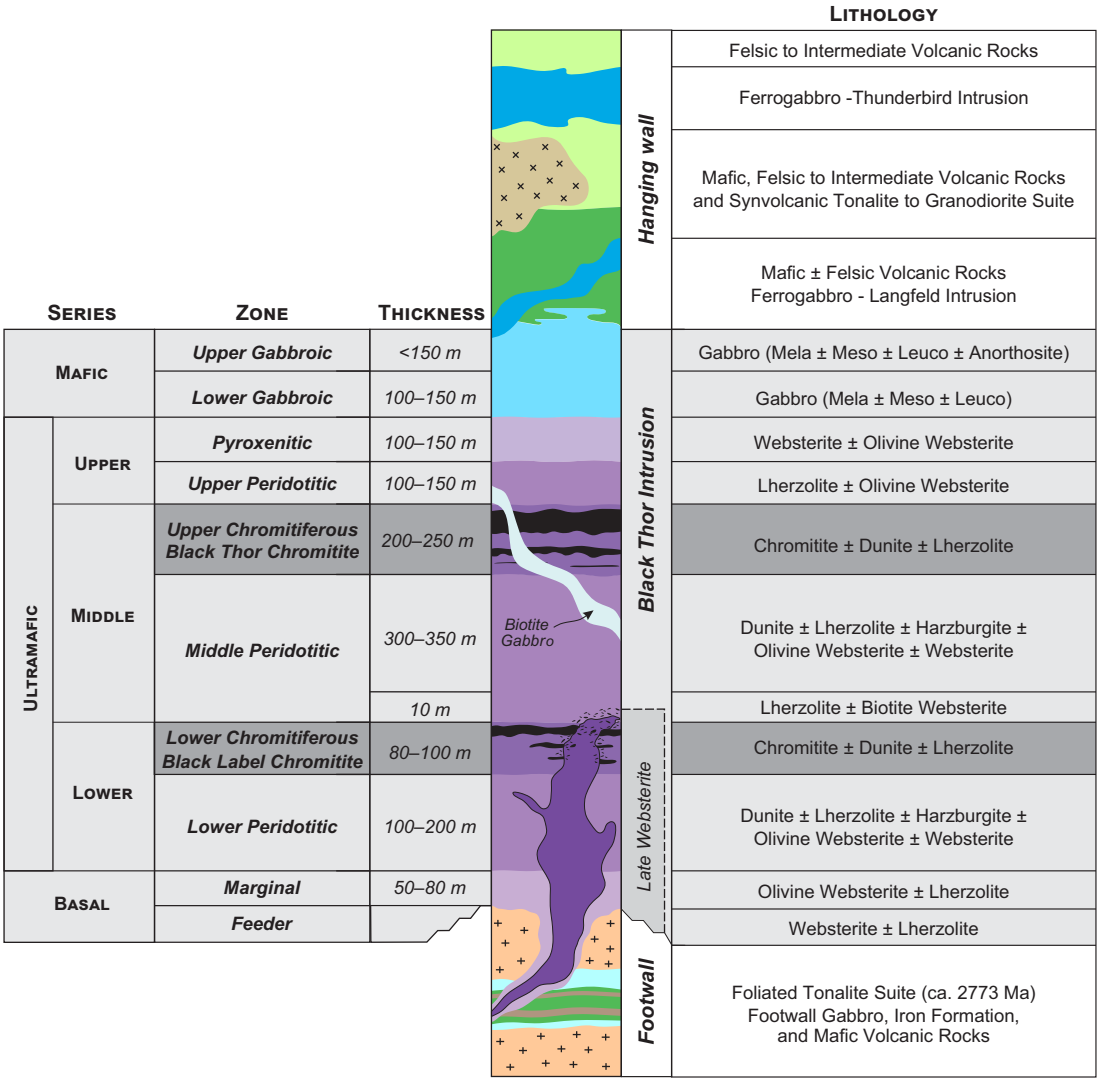

Figure 6. Idealized and schematic stratigraphic column of the Black Thor intrusion (Black Thor segment) in the Esker intrusive complex showing the various stratigraphic subdivisions (e.g. series and zones) and the confining lithological units of the footwall and hanging wall (*adapted from* Carson et al., 2015). Abbreviations: Leuco = leucogabbro; Mela = melagabbro, Meso = mesogabbro.

Mungall, 2018). South of the Frank Shear Zone, the Blackbird body is at least 1 km wide (east-west) and at least 700 m thick (north-south) between bounding faults (Fig. 5). To the north, the ultramafic body of AT-1 is interpreted to be the keel of the Double Eagle intrusion, where it is approximately 600 m wide (east-west) and 700 m thick (north-south) at its thickest. The ultramafic component of this intrusion is composed of variable proportions of dunite, harzburgite, and orthopyroxenite (Azar, 2010). There is little mafic component in this intrusion, except at the eastern end where it occurs as a thin layer approximately 100 m thick (north-south) at surface.

Eagle's Nest dyke

The Eagle's Nest dyke is a north-south-trending komatiitic ultramafic body with a flattened tube-shaped morphology that is interpreted to represent a structurally rotated subhorizontal blade-shaped dyke (Mungall et al., 2010; Zuccarelli et al., 2018a; Zuccarelli, in prep). In surface section (which approximates an original cross-section), it is ~500 m long (high) and ≤85 m wide (thick). The dyke has been drilled to a depth (length) of at least 1500 m. It is composed of an olivine-rich peridotite core flanked by more pyroxenitic margins (Zuccarelli et al., 2020; Zuccarelli, in prep). Mungall et al. (2010) described a marginal gabbro along parts of the contact, which might be explained by contamination and the presence of abundant xenoliths of country rocks (e.g. granodiorite, tonalite) in those areas. The ultramafic lithologies are mainly lherzolite, wehrlite, harzburgite, olivine pyroxenite, and pyroxenite that all contain orthopyroxene oikocrysts (Zuccarelli, in prep).

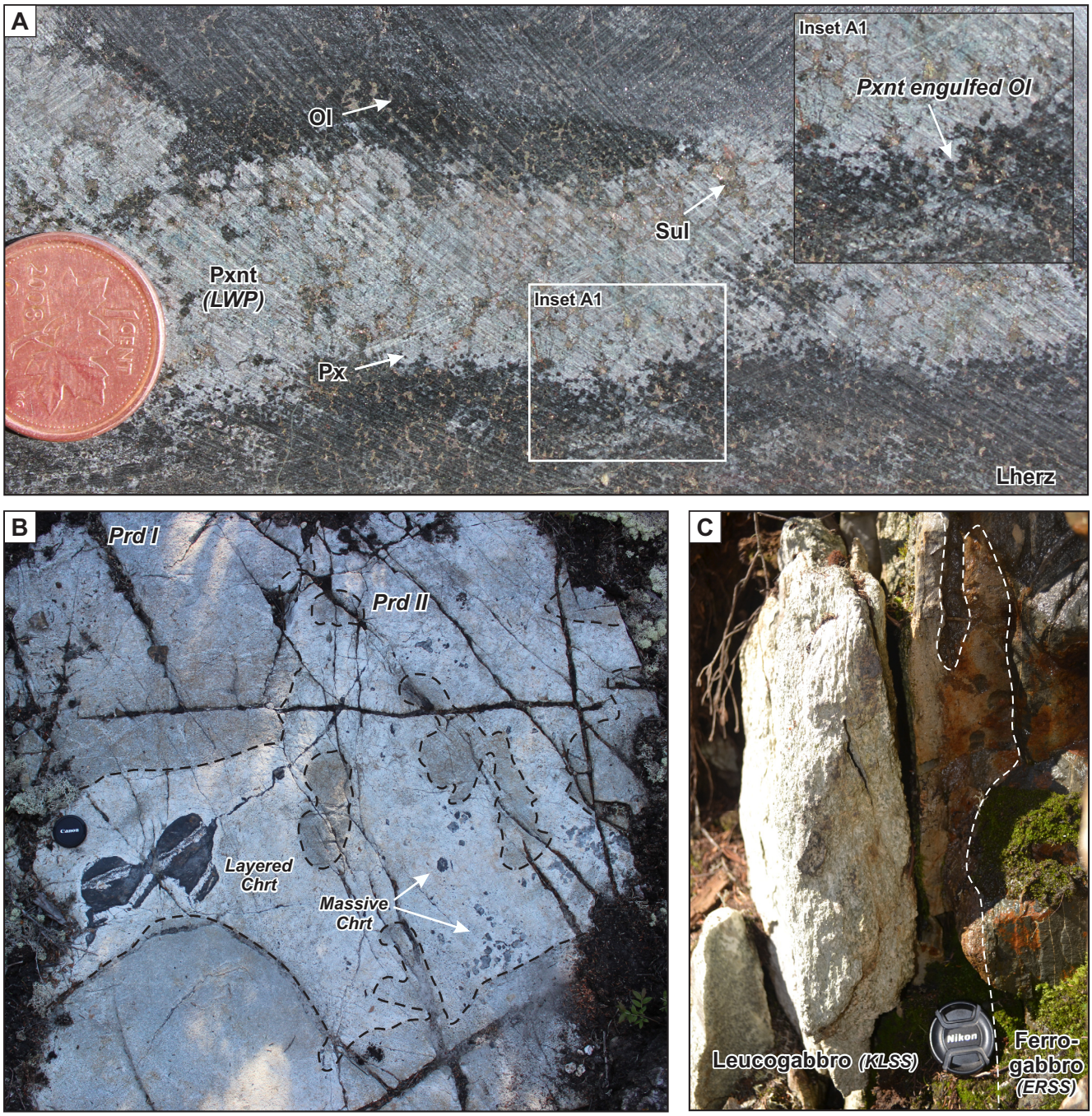

Figure 7. Field photographs showing some of the crosscutting relationships observed in the Black Thor intrusion within the Esker intrusive complex. **a)** Late Websterite phase injected into the lherzolite of the Black Thor intrusion. While the lherzolite was only partially unconsolidated, the pyroxenitic magma invaded the interstitial material, gradually engulfing the olivine crystals (*see* inset A1) of the lherzolite, producing hybrid rocks. Coin is 18 mm in diameter. **b)** Contact relationship between two peridotitic units in the Black Thor intrusion suggesting multi-generational emplacement of the komatiitic magma. Peridotitic unit II contains bimodal, subrounded to subangular chromitite inclusions: 1) numerous but small massive chromitite inclusions and 2) large but uncommon layered chromitite composed of massive chromitite and net-textured chromitite layers. Note that chromitite inclusions only occur within peridotitic unit II and are absent in peridotitic unit I. Lens cap is 6 cm in diameter. **c)** Iron- and titanium-enriched gabbroic dyke of the Ekwan River subsuite cutting leucogabbro (on the left) of the upper part of the Black Thor intrusion of the Koper Lake subsuite (KLSS). The white dashed line highlights the sharp intrusive contact between the two gabbroic rocks. Lens cap is 6 cm in diameter. Abbreviations: Chrt = chromitite; ERSS = Ekwan River subsuite; KLSS = Koper Lake subsuite; Lherz = lherzolite; LWP = Late Websterite phase; Ol = olivine; Prd I, Prd II = peridotitic unit, generation I and II, respectively; Px = pyroxene; Pxnt = pyroxenite; Sul = sulphide.

Other intrusive bodies

The C-6 intrusion is ~250 m wide (east-west) and ~750 m long (north-south) in surface section, narrowing and apparently terminating into the footwall rocks toward the north (Fig. 5) and cut off to the south by the Frank Shear Zone. It is poorly characterized but the magnetic signature combined with a few diamond drill core intersections suggests that it is composed mainly of ultramafic rocks.

The AT-5 intrusion is ~500 m wide (east-west) and up 650 m long (north–south) in surface section, narrowing and apparently terminating into the footwall rocks toward the north (Fig. 5). It consists mainly of peridotite to dunite with abundant relict igneous olivine (Fo_{91}–Fo_{86}: Houlé, unpubl. data), pyroxene, and subordinate gabbroic rocks.

Orthomagmatic Mineralization

Chromite mineralization correlation along strike

Chromite deposits are thus far restricted to the ultramafic-dominated Esker intrusive complex of the Koper Lake subsuite, which hosts at least six chromite deposits: the Black Thor, Black Label, Black Creek, and Big Daddy deposits in the Black Thor intrusion and the Black Horse, and Blackbird (including ore zones #1 and #2 referred as Blackbird 1 and Blackbird 2, respectively) deposits in the Double Eagle intrusion (Fig. 5). All six chromite deposits exhibit similar chromite textural facies, including finely disseminated, patchy disseminated, patchy net-textured, net-textured, semi-massive, and massive. These facies are commonly complexly interlayered, ranging from very thinly laminated (<1 mm) to very thickly bedded (>60 cm).

To aid in correlating the complex chromite-rich zones along strike, Laudadio (2019) subdivided them into (1) massive and semi-massive chromitite containing >35% Cr_2O_3 (~70 modal% chromite) and (2) disseminated, net-textured, and banded chromitite-dunite containing 15–35% Cr_2O_3 (~30–70 modal% chromite). Defined this way, the chromite mineralization within the Black Thor intrusion occurs as a relatively continuous and thick horizon that is broadly correlative over a strike length of 5 km. Mineralization up to 80 m thick occurs within the upper third of the Ultramafic Series, which is underlain by peridotitic units and overlain by olivine pyroxenitic to pyroxenitic units. Except for the Black Label Chromitite Zone that is predominantly composed of layered ore, all of the other chromitite zones (Black Thor, Black Creek, and Big Daddy) in the Black Thor intrusion consist of a relatively thin zone of massive and semi-massive chromitite surrounded by a thicker zone of disseminated, net-textured, and banded chromitite-dunite (Laudadio, 2019). In contrast, the main chromitite zones within the Double Eagle intrusion consist primarily of massive ores, although three layered chromitite horizons occur stratigraphically below the Blackbird 2 deposit (Laudadio, 2019).

Ni-Cu-(PGE) mineralization styles

Known Ni-Cu-(PGE) deposits are thus far also restricted to the ultramafic-dominated Esker intrusive complex of the Koper Lake subsuite. Only one deposit (Eagle's Nest) has geological resource estimates, but numerous Ni-Cu-(PGE) showings occur across the complex. Several types of Ni-Cu-(PGE) mineralization occur within the ultramafic component of the Esker intrusive complex (Farhangi et al., 2013; Houlé et al., 2015, 2017): 1) sulphide-rich conduit-style mineralization within feeder systems (e.g. Eagle's Nest, Blue Jay); 2) sulphide-rich contact-style mineralization along basal contacts (e.g. Black Thor intrusion Basal Contact, Blue Jay Extension); 3) sulphide-poor disseminated reef-style PGE-rich mineralization in chromitite horizons (e.g. Black Label, Black Thor); 4) sulphide-rich disseminated PGE-poor reef-style mineralization in fractionated gabbroic rocks in mafic zones (e.g. Black Thor intrusion); 5) sulphide-rich breccia mineralization associated with the emplacement of the slightly younger websteritic phase within the Black Thor intrusion (e.g. SW/Central/NE Breccia Zones); and 6) tectonically/hydrothermally mobilized sulphide-rich mineralization within shear zones (e.g. transition zone between ultramafic and mafic parts of intrusion; Fig. 5). More detailed work has been completed on these different types of mineralization at the Black Thor intrusion (Farhangi, in prep), and is currently ongoing at the Eagle's Nest deposit (Zuccarelli, in prep).

Summary

Although the mafic to ultramafic intrusive bodies of the Ring of Fire intrusive suite have similar emplacement/crystallization ages (Table 1; Houlé et al., 2015), they are significantly different in many respects: 1) the Koper Lake subsuite is spatially much more restricted than the Ekwan River subsuite (Fig. 1); 2) the Ekwan River subsuite does not contain any olivine-rich ultramafic rocks (Fig. 3); 3) the Koper Lake and Ekwan River subsuites show clear differences in their geochemical trends indicating a distinct geochemical evolution (Fig. 3); 4) the Ekwan River subsuite ferrogabbro locally crosscuts Black Thor leucogabbro (Fig. 7c), as well as other Koper Lake subsuite lithologies (evident in airborne magnetic maps), however, the opposite relationship is also observed locally in the Butler area; and 5) there are thin, highly deformed volcanic units between the Black Thor intrusion (i.e. Koper Lake subsuite) leucogabbro and Langfeld ferrogabbro (i.e.

Ekwan River subsuite; Fig. 5). Together, the above observations suggest discrete ultramafic-dominated (i.e. Koper Lake subsuite) and mafic-dominated (i.e. Ekwan River subsuite) intrusions with complex contact relationships, rather than a single, large, tectonically dismembered layered ultramafic-mafic intrusion, as previously suggested by Mungall et al. (2010).

DISCUSSION

Understanding the architecture of volcanic and intrusive plumbing systems of orthomagmatic mafic to ultramafic ore systems is critically important in determining their prospectivity and where chromite and Ni-Cu-(PGE) sulphide deposits might be located within these systems. However, the deposits and host units are normally small, making the task challenging, especially in deformed, metamorphosed, and glacially covered Archean greenstone belts like the McFaulds Lake greenstone belt.

Esker Intrusive Complex Structural Reconstruction

To improve our understanding of the plumbing systems of the Esker intrusive complex, a 3-D geological model was developed to better image the subsurface distribution and structural disposition of the Black Thor and the Double Eagle intrusions within the Esker intrusive complex (Laudadio et al., 2018a,b; Laudadio, 2019). The results mostly agree with the previous 2-D geological interpretation of Metsaranta and Houlé (2017b) but there are significant differences regarding the low-angle (i.e. to the stratigraphy) ductile shear zone (e.g. Frank Shear Zone) that transgresses the Esker intrusive complex subparallel to its internal stratigraphy (Fig. 5). The complex occurs entirely on the northern limb of a synform, so most of the stress appears to have been partitioned into these discrete low-angle shear zones (e.g. Frank Shear Zone and 3B Shear Zone), such that most of the ores and host rocks are not penetratively deformed and exhibit well preserved igneous textures. High-angle faults (i.e. to the stratigraphy) also transgress the complex but with apparent minor displacements (Fig. 5).

However, there are many features indicating that many—if not most—of the basal contacts of the Esker intrusive complex are primary features:

- Irregular contacts and hornfelsed footwall rocks along the basal contact of the Black Thor intrusion and at Eagle's Nest;
- Ultramafic protrusions extending from the ultramafic rocks into the footwall rocks at Eagle's Nest;
- Sulphide veinlets extending from mineralized peridotite into the footwall rocks at Eagle's Nest and the Basal Contact Zone of the Black Thor intrusion;
- The connection between the Basal Series of the AT-12 keel and the overlying Lower Ultramafic Series of the Black Thor intrusion;
- The continuity between the Late Websterite phase in the AT-12 keel and the Lower Ultramafic Series of the Black Thor intrusion; and
- The presence of mineralogically and geochemically similar Ni-Cu-(PGE) mineralization at Blue Jay, Blue Jay Extension, and Basal Contact Zone within the Black Thor intrusion.

At the northeast end of the complex, in the Black Thor intrusion, the amount of dextral displacement along the 3B Shear Zone is not well known, but it is inferred to be minimal based on a lack of offset along the geophysically interpreted contacts of the Langfeld intrusion but also by the apparent continuity of units on both side of the 3B Shear Zone within the Esker intrusive complex (Fig. 4, 5). Nonetheless, only within the northernmost part of the intrusion, the chromite horizon appears to be structurally repeated along 3B Shear Zone, roughly parallel to the stratigraphy (Tuchscherer et al., 2010). Conversely, at the opposite end of the complex, the C-6, AT-5, and AT-1 keels on the northwest side of the Frank Shear Zone are displaced from the Double Eagle and AT-3 chonoliths (Fig. 4). The conceptual restoration of deformation by Laudadio (2019) suggests dextral displacement of 1 to 1.5 km along the Frank Shear Zone. This would connect the AT-1 and Blackbird bodies to form the Double Eagle intrusion, and reconnect the gabbro units between the Black Thor and Double Eagle intrusions, which would bring the Double Eagle and AT-3 intrusions closer to the Black Thor intrusion (Fig. 4). However, this interpretation leaves the C-6 and AT-5 keels "stranded" with little or no overlying ultramafic components on the southeast side of the shear zone. An alternative scenario involves 3 to 4 km of dextral displacement along the Frank Shear Zone, which would connect C-6 with the Double Eagle complex, and AT-5 and AT-1 with AT-3 (*see* Fig. 4). Both scenarios support a linkage between the Black Thor and Double Eagle intrusions and their assignment to a single intrusive complex, as was proposed by Houlé et al. (2019).

Regardless of the magnitude of displacement along the Frank Shear Zone, the 3-D reconstruction of the Esker intrusive complex suggests that the Eagle's Nest dyke is not directly connected (Laudadio, 2019) and may therefore not be the magma conduit of the Double Eagle intrusion. We cannot completely rule out additional structural complexity as an explanation for this spatial relationship between these bodies, but this interpretation is supported by the much greater abundance of Fe-Ni-Cu sulphides in the Eagle's Nest dyke and the much greater abundance of chromite in the Double

Eagle intrusion, requiring an "upstream" (lateral or deeper) source for the rare chromitite clasts within the Eagle's Nest dyke (*see* the discussion about Ore Genetic Models; Zuccarelli et al., 2020).

Similarly, although the ~90º east-southeast structural rotation is well defined by younging directions inferred from textural, mineralogical, and lithogeochemical gradations in the Eagle's Nest dyke, Double Eagle intrusion, and Black Thor intrusion, the estimate of fault displacement relies heavily on geophysics and may require revision after more geological data about the relationship between the Double Eagle and the Black Thor intrusions become available.

Magmatic Architecture of the Esker Intrusive Complex

After removal of the superimposed deformation, the Esker intrusive complex consists of a semi-continuous sill-like ultramafic±mafic body that incorporates the Double Eagle transitional dyke/chonolith, which is underlain by the keel-shaped AT-1, AT-5, and C-6 bodies and the Eagle's Nest dyke (Fig. 8). It also contains the trough-shaped Black Thor sill, which is underlain by the keel-shaped AT-12 body.

All of the keel-shaped intrusive bodies along the north-northwest margin of the Esker intrusive complex appear to have been originally oriented at >60º to the basal contact of the Esker intrusive complex, emplaced along inferred synvolcanic faults, and thin rapidly northward, suggesting that they were all originally subhorizontal to slightly inclined blade-shaped dykes similar to unmineralized (e.g. Hawaii: Rubin and Pollard, 1987; New Zealand: Shelley, 1988) and mineralized (e.g. Expo-Méquillon: Mungall, 2007; Savannah: Barnes et al., 2016; Huangshan, Jinchuan, Jingbulake, Kalatongke #1, Hongqiling #1, Limahe, Qingkuangshan, Zhubu: Lu et al., 2019; *see* review by Lesher, 2019) subhorizontal dykes in many other subvolcanic systems. These keel-like bodies are interpreted to have fed the overlying Black Thor and Double Eagle intrusions. Subhorizontal blade-shaped dykes are interpreted to form at a level of neutral buoyancy (e.g. in this case near the contact between the less dense granitoid rocks and the denser mafic±felsic volcanic rocks and iron formations) in an extensional stress regime that facilitates lateral propagation (e.g. Rubin and Pollard, 1987; Townsend et al., 2017). The clear connections between the AT-12 and AT-1 intrusions and the overlying Black Thor and Double Eagle intrusions, respectively, suggest that over time the upper parts of the bladed dykes intruded laterally and expanded (as shown in the experiments by Kavanagh et al., 2015) to form a transitional dyke/chonolith (Double Eagle intrusion) and a trough-shaped sill (Black Thor intrusion). The Double Eagle and Black Thor intrusions are interpreted to have eventually coalesced to form the Esker intrusive complex (Fig. 8; Houlé et al., 2019; *see* discussion by Magee et al., 2016; Biggs and Annen, 2019). Thus, the Esker intrusive complex appears to preserve all components of the transition from bladed dykes through chonoliths to channelized sills.

Regardless of the mechanism and timing of growth and coalescence, Ni-Cu-(PGE) mineralization was localized in environments of linear propagation (blade-shaped dykes), whereas chromite mineralization was localized in environments of transitional (chonoliths) and subhorizontal (trough-shaped sill) propagation.

System Dynamics

Komatiite-associated Ni-Cu-(PGE) deposits form in high-flux lava channels, channelized sheet flows, chonoliths, and channelized sheet sills (e.g. Lesher et al., 1984; Lesher, 1989, 2017, 2019; Barnes, 2006; Lesher and Barnes, 2009; Barnes et al., 2016) and it is now recognized that some types of stratiform chromite deposits formed in similar environments (e.g. Prendergast, 2008; Lesher et al., 2019).

Ni-Cu-(PGE) ores typically occur at or near the base of their host units, suggesting that they form early, prior to the crystallization of the overlying rocks, which are typically olivine±pyroxene cumulates. Overlying olivine-rich cumulate rocks indicate continued high magma fluxes, whereas differentiation to more evolved gabbroic rocks indicates waning magma fluxes (e.g. Lesher and Keays, 2002). The ores are sometimes coarsely layered (e.g. Raglan: Lesher, 2007; Alexo: Houlé et al., 2012), but never finely layered and are commonly just zoned (e.g. Kambalda: Ewers and Hudson, 1972). The Ni-Cu-(PGE) ores at Eagle's Nest are overlain by barren peridotites and lesser pyroxenites, consistent with continued high magma fluxes, and have complexly zoned net-textured subfacies, but are not layered (Zuccarelli et al., 2020; Zuccarelli, in prep).

In contrast, Cr deposits occur above the base of the host units and are typically finely interlayered with barren or weakly mineralized olivine±pyroxene cumulate rocks. The origin of the layering is not well understood but is normally interpreted to reflect some combination of multiple influxes ± magma mixing (*see* review by Namur et al., 2015) rather than continuous or semi-continuous high-flux flow. Although both deposits form in dynamic systems, it appears that high-grade conduit-hosted Ni-Cu-(PGE) deposits form at higher magma fluxes than high-grade conduit-hosted Cr deposits.

It is not yet clear whether the sulphides and oxides in the Esker intrusive complex formed at more-or-less the same time in different environments under different fluid dynamic conditions (higher flux blade-shaped

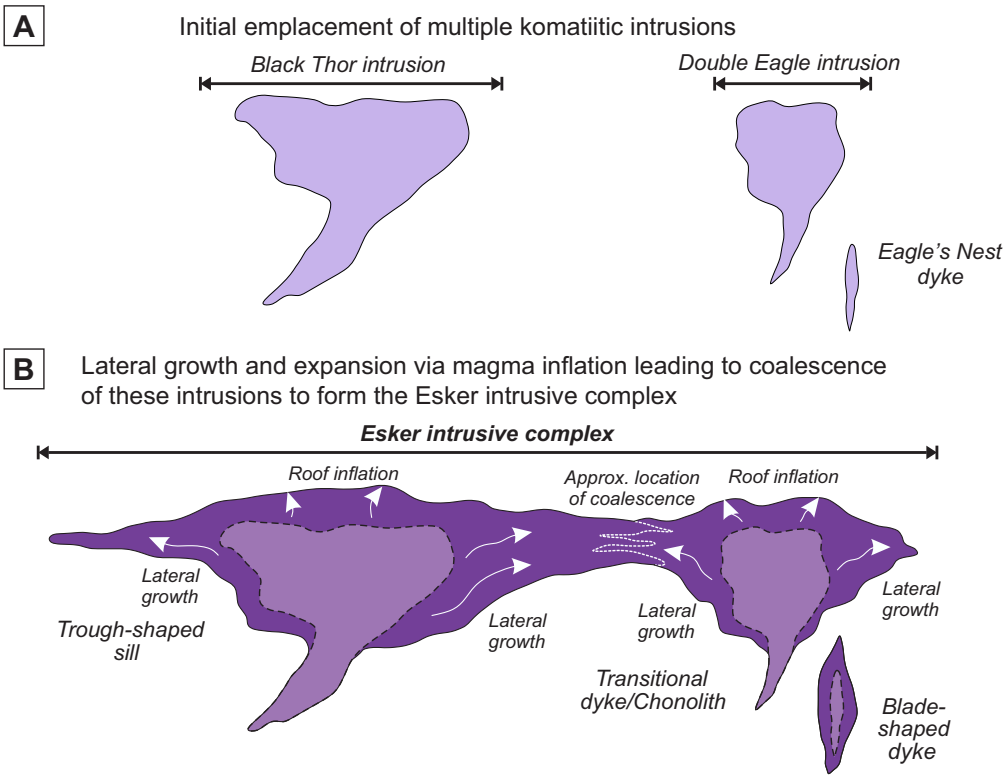

Figure 8. Schematic reconstruction (not to scale) of the evolution of the Esker intrusive complex (*modified from* Houlé et al., 2019). **a)** The light purple represents the initial individual emplacement of the Black Thor and Double Eagle intrusions and the Eagle's Nest dyke. **b)** The continuation of magma flux through each system resulted in the vertical inflation and lateral expansion of the Black Thor and the Double Eagle intrusions until eventually they coalesced to form the Esker intrusive complex. The dark purple represents the full extent of the intrusions that form the Esker intrusive complex; medium purple represents the trace of the initial magma bodies emplaced in (a). The white arrows indicate the displacement of magma throughout the inflation processes; the white dashed line indicates the approximate location of the coalescence of the Black Thor and Double Eagle intrusions. Not shown in this diagram is the Frank Shear Zone, which subsequently faulted the Esker intrusive complex. Note that for simplicity, the late websteritic phase has been omitted from this schematic reconstruction.

dykes versus lower flux channelized sills) or whether they formed at different times as the geometries and fluid dynamic conditions evolved within the system (higher flux blade-shaped dykes evolving into lower flux channelized sills). Additional U-Pb dating might be helpful to establish the geochronological relationships among the different intrusion types and whether any age gradation can be observed.

Ore Genesis

Magmatic chromite deposits

The chromite deposits in the McFaulds Lake greenstone belt of the Ring of Fire region do not exhibit the main geological characteristics of traditional stratiform deposits hosted by large periodically replenished magma chambers. They are considered to be part of a subtype hosted by smaller magmatic conduits (e.g. Prendergast, 2008; Lesher et al., 2019). One fundamental problem in the genesis of all stratiform chromite deposits is how layers of massive to semi-massive chromitite that are commonly up to 1 m thick (e.g. Bushveld Complex–South Africa; Stillwater Complex–USA; or Great Dyke–Zimbabwe), sometimes up to 10 m thick (e.g. Inyala and Railway Block–Zimbabwe; Ipueira-Medrado–Brazil; Uitkomst–South Africa; and Sukinda–India), and less commonly up to 100 m thick (e.g. Kemi–Finland; Esker intrusive complex–Canada) are generated from magmas that typically contain <0.35% Cr and crystallize very small amounts of chromite (normally <1 modal% of the cumulus assemblage; see discussion by Lesher et al., 2019). Although many models have been suggested over the years (see discussion by Lesher et al., 2019), and even if most of the suggested processes could have operated alone or in combination to generate thin layers of semi- to massive chromitites, none of these appear capable of generating the vast amounts of chromite that are present in the Esker intrusive complex relative to its preserved size. To solve this mass balance problem, Lesher et al. (2019) proposed a process involving partial melting of Fe±Ti oxide-rich rocks (oxide-facies iron formation or ferrogabbro) and conversion of fine-grained xenocrystic oxide to chromite by reaction with Cr-rich komatiitic magma in a dynamic magma conduit (Fig. 9). They demonstrated that this process was geologically, physically, and chemically feasible, and suggested that it

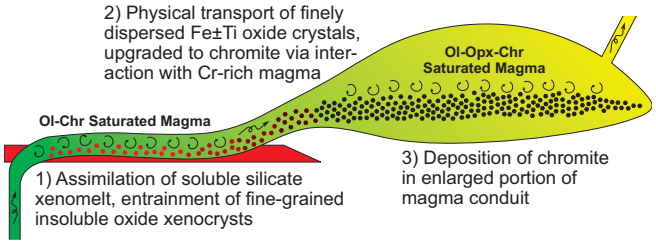

Figure 9. Schematic model of the dynamic upgrading of Fe±Ti oxides derived from oxide-facies iron formation or ferrogabbro via interaction with Cr-rich komatiitic magma (Lesher et al., 2019). Abbreviations: Chr = chromite, Ol = olivine, Opx = orthopyroxene.

probably occurred in the Black Thor intrusion.

Lesher et al. (2019) assumed that the magmas were saturated in chromite and could not dissolve significant amounts of xenocrystic magnetite or ilmenite from footwall oxide-facies iron formations or gabbros. Experiments by Keltie (2018) and MELTS models (Azar, 2010; Carson, in prep) suggest that high-Mg komatiites are able to assimilate significant amounts of magnetite (as much as 66 wt% FeO in the Keltie experiments) before saturating the komatiitic magma in magnetite. However, this seems difficult to reconcile with the worldwide paucity of Fe-rich komatiites (other than geochemically and isotopically distinct ferropicrites) and the presence of oxide-facies iron formation xenoliths within the Double Eagle intrusion (Blackbird deposit: Azar, 2010), the Black Thor intrusion (Carson et al., 2016; Carson, in prep), and elsewhere (e.g. Perring et al., 1995, 1996; Prendergast, 2001). Establishing the Fe contents of liquids that formed rocks containing cumulus olivine±chromite±orthopyroxene assemblages with negligible trapped liquid components is difficult, but relict igneous olivine compositions in the Black Thor intrusion range up to Fo_{94} (Laarman, 2014) and there is a subset of high-Mg, low-Fe peridotites in the Black Thor intrusion that must contain olivine ranging up to that composition (Carson, in prep). This olivine composition is similar to the most magnesian olivine in the Alexo komatiite of the Abitibi greenstone belt, which is inferred to have crystallized from a liquid containing ~28 wt% MgO and ~11 wt% FeO_{total} (Arndt, 1986). Many Black Thor cumulate rocks crystallized from more evolved magmas with higher Fe and lower Mg contents (Carson, in prep), but it is unlikely that the high-Mg olivine or high-Mg, low-Fe cumulate rocks crystallized from magmas with higher Fe contents, as this would require the magma to have proportionally higher Mg contents. Thus, the olivine and whole-rock data suggest a typical high-Mg, moderate-Fe komatiitic parental magma that evolved through a combination of fractional crystallization± assimilation of iron-formation to higher Fe, lower Mg compositions.

Table 2. Comparison of the characteristics of the mechanical sorting of the cotectic olivine-chromite crystallization model and the Fe±Ti oxide xenocryst upgrading model

	Mechanical Sorting of Cotectic Ol-Chr	Dynamic Upgrading of Fe±Ti Oxide Xenocrysts
V–Ga abundances and trends (and overall limited range in chromite compositions)	yes	yes
Composite chromite-silicate-sulphide grains containing Fe±Cu sulphides *(Ni-absent)* that are texturally and mineralogically similar to interlayered massive magnetite-silicate-sulphide (Fe±Cu) in the footwall iron formation	no	yes
Absence of proportionally (50x) large amounts of olivine cumulate rocks	no	yes
High solubility of Fe±Ti oxide in komatiite melt	yes	no

Abbreviations: Chr = chromite, Ol = olivine.

Brenan et al. (2019) showed that the V and Ga contents of Black Thor chromite are consistent with crystallization of olivine and chromite in more-or-less cotectic proportions (50:1), not with crystallization of olivine alone (which would produce higher V/Ga ratios) or of significant amounts of chromite (which would produce lower V/Ga ratios). These observations led Brenan et al. (2020) to propose that the chromite deposits within the Esker intrusive complex formed by cotectic crystallization of olivine-chromite, followed by subsequent crystal sorting, a variant of the H_2O-addition mechanical-sorting model proposed by Azar (2010).

A detailed evaluation of the two models is beyond the scope of this contribution and will be addressed by Carson (in prep), but a preliminary comparison of the ability of the models to explain some of the geological, textural, mineralogical, and geochemical observations are summarized in Table 2. There are several key points that should be considered.

- Both models can explain the abundances and broadly positive correlation between V and Ga in the Ring of Fire chromite. In the case of the xenocryst-upgrading model, V (*see* Lesher et al., 2019) and Ga increase with magma:oxide ratio and reach the observed levels at high magma:oxide and oxide: olivine ratios, provided that the initial V and Ga contents in the magma are similar to those of the most fractionated magma required in the cotectic fractionation model (Carson, in prep). A minor technical point is that fractional crystallization± assimilation models do not make allowances for diffusion, which Lesher et al. (2019) showed would be very rapid for such small (<0.2 mm) grain sizes. This results in a physical-chemical process more similar to equilibrium crystallization, which would reduce the degrees of fractionation in

the models to some degree and require higher initial V and Ga contents in the magma or higher chromite/melt partition coefficients to achieve the same enrichments.

- Both models can explain the massive and silicate melt inclusion-bearing chromite types (e.g. Carson et al., 2015), but only the xenocryst-upgrading model can explain the minor but significant Fe±Cu sulphide-bearing chromite grains within massive to disseminated chromite-rich lithofacies in the Black Thor intrusion, which closely match the textures and sulphide mineralogy of footwall iron formations (Carson et al., 2015, 2016; Lesher et al., 2019). Importantly, the absence of pentlandite as a component of the sulphide inclusions in the chromite grains indicates that the sulphide inclusions did not segregate from the komatiitic magma, as did other sulphides in the Esker intrusive complex (e.g. Eagle's Nest, Blue Jay, Blue Jay Extension, Black Label Breccia Zone: Farhangi et al., 2013; Zuccarelli et al., 2020).
- Azar (2010) and Brenan et al. (2019, 2020) did not indicate whether the proposed mechanical sorting process occurred below, within, or above the Esker intrusive complex, but a cotectic olivine-chromite crystallization and mechanical segregation model requires the production of 50x more olivine than chromite. The Black Thor intrusion does not contain significant amounts of excess olivine (Carson, in prep), so this model requires the formation of 50x larger or 50x more numerous barren dunite bodies (or larger or more numerous peridotite bodies), which have not been observed thus far in the Ring of Fire region, or in any of the other localities where deposits of this type occur. Alhough the Ring of Fire region is poorly exposed, such units should stand out on regional magnetic surveys, which does not appear to be the case. Similarly, the olivine-rich units could also have been eroded or structurally removed (e.g. McFaulds Shear Zone), but one would expect at least some of such large volumes of dunite to be preserved.
- A xenocryst-upgrading model is not consistent with the high solubility of magnetite predicted by MELTS models (Azar, 2010; Carson, in prep) and the Keltie (2018) experiments, and the moderate FeO_T contents of the parental magma. The high magma:oxide values inferred by Lesher et al. (2019) would dilute the effects of assimilation (*see* Lesher et al., 2001), but this would also maintain solubility.

At this stage both models have at least one serious deficiency (*see* Table 2) that must be reconciled to adequately explain the genesis of thick chromitite zones. In our opinion, the observed composite chromite-silicate-sulphide grains provide unambiguous evidence of an oxide-silicate-sulphide source for at least some of the chromite; we are presently evaluating explanations for the magnetite solubility.

Magmatic Ni-Cu-PGE deposits

The main ingredients required for the generation of high-grade magmatic Ni-Cu-PGE sulphide deposits appear to be (1) sulphide-undersaturated magmas derived by moderate to high degrees of melting of peridotitic or pyroxenitic asthenospheric mantle (e.g. Keays, 1982; Lesher and Stone, 1996; Arndt et al., 2005; Lu et al., 2019); (2) an external source of S (e.g. Lesher and Groves, 1986; Lesher and Campbell, 1993; Keays and Lightfoot, 2010; Ripley and Li, 2013); (3) a high-flux magma conduit (lava channel, channelized sheet flow, chonolith, channelized sheet sill) to facilitate thermomechanical erosion (e.g. Huppert et al., 1984; Lesher et al, 1984); and (4) a favourable site of deposition (e.g. Barnes et al., 2016; Lesher, 2017, 2019).

The Eagle's Nest deposit, the only known high-grade Ni-Cu-(PGE) deposit in the Ring of Fire region, exhibits all of these features (Zuccarelli, in prep). Although most of these features are also present in other parts of the Esker intrusive complex but, as noted above, most other parts (Black Thor and Double Eagle intrusions) appear not to have had high magma fluxes, which may explain why they contain only minor Ni-Cu-(PGE) sulphides (e.g. Black Thor intrusion: Farhangi, in prep).

The ^{34}S isotopic compositions of the Ni-Cu-(PGE) mineralization within the Esker intrusive complex (-3 to +2‰ $\delta^{34}S$; Farhangi, in prep) are much more variable than mantle values (0.1 ± 0.5‰; Sakai et al., 1982, 1984) but overlap footwall iron formation (-1 to +1.5‰ $\delta^{34}S$; Carson, in prep). These overlapping values suggest that footwall oxide-sulfide-silicate iron formations are a potential source for most of the S in the system. The amount of sulfide in the iron formations examined thus far is limited, so additional sources such as sulphidic graphitic argillites, should also be considered, but their distribution and abundance is poorly constrained at this stage.

IMPLICATIONS FOR EXPLORATION

Our knowledge in the Ring of Fire region has increased significantly since the beginning of collaborative efforts between the Geological Survey of Canada, the Ontario Geological Survey, academia, and industry partners under the Targeted Geoscience Initiative (Phases 4 and 5). Some guidelines are listed below that could help target the most prospective areas for orthomagmatic mineralization across the Superior Province.

- At the craton-scale, the well endowed McFaulds Lake greenstone belt lies within the Oxford-Stull domain, which is part of the larger Bird River–Uchi–Oxford-Stull–La Grande Rivière–Eastmain superdomain. It defines a large metallotect that is highly prospective for orthomagmatic Cr, Ni-Cu-PGE and Fe-Ti-V (Houlé et al., 2015, 2020).
- At the greenstone belt-scale, the regionally mappable Muketei assemblage is, thus far, the most prospective part recognized thus far, of the McFaulds Lake greenstone belt, as it hosts not only all of the known orthomagmatic Cr-(PGE), Ni-Cu-(PGE), and hydrothermal VMS deposits, but also significant orthomagmatic Fe-Ti-V prospects and orogenic gold mineralization (Metsaranta et al., 2015; Houlé et al., 2020; Metsaranta and Houlé, 2020).
- At the district-scale, almost all of the orthomagmatic deposits in the Ring of Fire region are intimately related to a large mafic to ultramafic magmatic event, recognized as the Ring of Fire intrusive suite, which is known to have been emplaced in a very restricted time between 2736 and 2732 Ma.
    - Ultramafic-dominated intrusions of the Koper Lake subsuite are the prime target for Cr and Ni-Cu-(PGE) mineralization.
    - Mafic-dominated intrusions of Ekwan River subsuite are the prime target for Fe-Ti-V mineralization.
- At the scale of an individual intrusive complex, the Esker intrusive complex
    - Comprises multiple discrete coeval and comagmatic intrusive bodies,
        - some of which contain high-grade, high-tonnage Ni-Cu-(PGE) mineralization (e.g. Eagle's Nest dyke),
        - some of which contain high-grade, high-tonnage Cr mineralization (e.g. Double Eagle and Black Thor intrusions).
        - which appears to have been initially emplaced as separate intrusions that coalesced over time through lateral growth and magma inflation within a dynamic komatiitic system.
    - Is a mafic to ultramafic ore system in which all the deposits recognized thus far, were originally subhorizontal and subconcordant to the regional stratigraphy.
        - Ni-Cu-(PGE) mineralization occurs predominantly within the very high magma flux and highly dynamic blade-shaped dykes of the system (e.g. Eagle's Nest).
        - Cr-(PGE) mineralization occurs predominantly within the high magma flux but slightly less dynamic transitional dykes/chonoliths (e.g. Double Eagle intrusion) to through-shaped sills (e.g. Black Thor intrusion) of the system.
        - Despite the strong association between mineralization and the host geometries, we cannot preclude that other mineralization could be found in other parts of the system given that the Esker intrusive complex is seen as having a complete continuum in their host geometry and also in their mineralization.

The wide diversity of mineral deposit types in the McFaulds Lake greenstone belt, and especially the Cr-(PGE), Ni-Cu-(PGE), and Fe-Ti-V-(P) mineralization related to mafic to ultramafic rocks, make the Ring of Fire region an unmatched exploration target of emerging world-wide economic importance as a source for critical minerals.

ONGOING AND FUTURE WORK

A little more than a decade ago, the Ring or Fire region was poorly known and did not represent a prime mineral exploration target within the Superior Province, even less so for orthomagmatic Ni-Cu-(PGE), Cr-(PGE) or Fe-Ti-V-(P) mineralization. Despite slow development, this region of the Superior Province is now regarded as one of Canada's future mining camps. Significant progress in our understanding of this mineralized system has been made in recent years as part of the Targeted Geoscience Initiative (TGI). There are, however, many unresolved questions that merit further research.

This contribution offers a current summary of some of the critical advances made over the years during the TGI program. A few graduate studies at Laurentian University (H.J.E. Carson, Ph.D candidate – Black Thor intrusion; N. Zuccarelli, M.Sc. candidate – Eagle's Nest deposit; and K. Kuster, Ph.D. candidate – Geochemical modelling of the Esker intrusive complex) are on-going. Furthermore, numerous contributions on various aspects of the Ring of Fire are currently underway, in addition to Ontario Geological Survey Open File report summarizing the regional mapping work conducted by the OGS in collaboration with the GSC Targeted Geoscience Initiative during the past decade (Metsaranta and Houlé, 2020).

ACKNOWLEDGMENTS

This report is a contribution to NRCan's Targeted Geoscience Initiative (TGI) Program. Support for this study was provided through the Orthomagmatic Ni-Cu-PGE-Cr Ore Systems Project's 'Activity NC-2.1: Architecture of magmatic conduits in Cr-(PGE)/Ni-Cu-

(PGE) ore systems' and has benefitted from financial support by NSERC and Cliffs Natural Resources (CRDPJ 446109 – 2012).

We are grateful to Noront Resources Ltd., Cliffs Natural Resources/Freewest Resources, KWG Resources Inc., MacDonald Mines Ltd., Fancamp Exploration Ltd., Bold Ventures Inc., Probes Mines, UC Resources, and Canterra Minerals for their generous assistance, providing access to properties, and permission to access diamond-drill cores and corporate geological databases over the years. We also greatly appreciated the involvement and participation of numerous researchers Pete Hollings (Lakehead University), Jim Mungall (Carleton University), and Claire Samson (Carleton University) and students (Naghmeh Farhangi, Ben Kuzmich, Jordan Laarman, Kaveh Merhmanesh, C.J. Spath, and Natascia Zuccarelli) from the Ring of Fire Targeted Geoscience Initiative research group that have facilitated advances in our understanding of the Ring of Fire geology. We are grateful to Nicole Rayner (GSC-Ottawa) for providing high-quality geochronological analysis throughout the TGI-5 program over the years. Furthermore, we express our appreciation to numerous academic researchers and mining company geologists for geological discussions over the years, but especially geologists of Cliffs Natural Resources (Richard Fink, Andrew Mitchell, Michael Orobona, Ryan Weston, and David Shinkle) and Noront Resources (Ryan Weston, Matt Downey, Stephen Flewelling, Matt Deller, and Geoff Heggie) and KWG Resources (Moe Lavigne). This report benefited from the scientific review of Martin Tuchscherer (Tascan Geosciences Inc.), and Wouter Bleeker (GSC) and editorial review by Elizabeth Ambrose and Valérie Bécu (GSC).

REFERENCES

Arndt, N.T., 1986. Differentiation of komatiite flows; Journal of Petrology, v. 27, p. 279–303.

Arndt, N.T., Lesher, C.M., and Czamanske, G.K., 2005. Mantle-derived magmas and magmatic Ni-Cu-(PGE) deposits; *in* Economic Geology 100th Anniversary Volume, (ed.) J.W. Hedenquist, J.F.H. Thompson, R.J. Goldfarb, and J.P. Richards; Society of Economic Geologists, p. 5–23.

Azar, B., 2010. The Blackbird chromite deposit, James Bay Lowlands of Ontario, Canada: Implications for chromitite genesis in ultramafic conduits and open magmatic systems; M.Sc. thesis, University of Toronto, Toronto, Ontario, 154 p.

Barnes, S.J., 2006. Komatiite-hosted nickel sulfide deposits: geology, geochemistry, and genesis; Chapter 3 *in* Nickel Deposits of the Yilgarn Craton: Geology, geochemistry, and geophysics applied to exploration, (ed.) S.J. Barnes; Society of Economic Geologists, Special Publication 13, p. 51–97.

Barnes, S.J. and Mungall, J.E., 2018. Blade-shaped dikes and nickel sulfide deposits: A model for the emplacement of ore-bearing small intrusions; Economic Geology, v. 113, p. 789–798.

Barnes, S.J., Cruden, A.R., Arndt, N.T., and Saumur, B.M., 2016. The mineral system approach applied to magmatic Ni-Cu-PGE sulphide deposits; Ore Geology Reviews, v. 76, p. 296–316.

Biggs, J. and Annen, C., 2019. The lateral growth and coalesence of magma systems; Royal Society A: Mathematical, Physical and Engineering Sciences, Philosophical Transactions, v. 377, 20180005, p. 1–20.

Brenan, J.M., Woods, K., Mungall, J.E., and Weston, R., 2019. Origin of chromitites in the Ring of Fire Part II: Trace element fingerprinting of contaminants; *in* Targeted Geoscience Initiative 5 Grant Program interim reports 2018–2019, (ed.) K.U. Rempel, A.E., Williams-Jones, and K. Fuller; Geological Survey of Canada, Open File 8620, p. 5–18.

Brenan, J.M., Woods, K., Mungall, J.E., and Weston, R., in press. Origin of chromitites in the Ring of Fire intrusive suite as revealed by chromite trace element chemistry and simple crystallization models; *in* Targeted Geoscience Initiative 5: Grant program final reports (2018–2020); Geological Survey of Canada, Open File 8734.

Carson, H.J.E., in prep. Stratigraphy, geochemistry, and petrogenesis of the Black Thor intrusion and associated Cr and Ni-Cu-PGE mineralization, McFaulds greenstone belt, Ontario; Ph.D. thesis, Laurentian University, Sudbury, Ontario.

Carson, H.J.E., Lesher, C.M., and Houlé, M.G., 2015. Geochemistry and petrogenesis of the Black Thor intrusive complex and associated chromite mineralization, McFaulds Lake greenstone belt, Ontario; *in* Targeted Geoscience Initiative 4: Canadian Nickel-Copper-Platinum Group Elements-Chromium Ore Systems—Fertility, Pathfinders, New and Revised Models, (ed.) D.E. Ames and M.G. Houlé; Geological Survey of Canada, Open File 7856, p. 87–102.

Carson, H.J.E., Lesher, C.M., and Houlé, M.G., 2016. Oxide chemostratigraphy of the Black Thor Chromitite Zone, Black Thor Intrusive Complex, McFaulds Lake, Canada; Geological Survey of Western Australia, 13th International Ni-Cu-PGE Symposium, Abstracts, Record 2016/13, p. 19.

Ewers, W.E. and Hudson, D.R., 1972. An interpretive study of a nickel-iron sulfide ore intersection, Lunnon shoot, Kambalda, Western Australia; Economic Geology, v. 67, p. 1075–1092.

Farhangi, N., in prep. Mineralogy, geochemistry, and petrogenesis of Ni-Cu-(PGE) mineralization in the Black Thor intrusion, McFaulds Lake greenstone belt, Ontario; M.Sc. thesis, Laurentian University, Sudbury, Ontario.

Farhangi, N., Lesher, C.M., and Houlé, M.G. 2013. Mineralogy, geochemistry and petrogenesis of nickel-copper-platinum group element mineralization in the Black Thor Intrusive Complex, McFaulds Lake greenstone belt, Ontario; *in* Summary of Field Work and Other Activities, 2013; Ontario Geological Survey, Open File Report 6290, p.55-1 to 55-7.

Houlé, M.G., Lesher, C.M., and Davis, P.C., 2012. Thermo-mechanical erosion and genesis of komatiite-associated Ni-Cu-(PGE) mineralization at the Alexo Mine, Abitibi Greenstone Belt, Ontario; Mineralium Deposita, v. 47, p. 105–128.

Houlé, M.G., Lesher, C.M., McNicoll, V.J., Metsaranta, R.T., Sappin, A.A., Goutier, J., Bécu, V., Gilbert, H.P., and Yang, X.M., 2015. Temporal and spatial distribution of magmatic Cr-(PGE), Ni-Cu-(PGE), and Fe-Ti-(V) deposits in the Bird River–Uchi–Oxford-Stull–La Grande Rivière–Eastmain domains: A new metallogenic province within the Superior Craton; *in* Targeted Geoscience Initiative 4: Canadian Nickel-Copper-Platinum Group Elements-Chromium Ore Systems —Fertility, Pathfinders, New and Revised Models, (ed.) D.E. Ames and M.G. Houlé; Geological Survey of Canada, Open File 7856, p. 37–48.

Houlé, M.G., Lesher, C.M., McNicoll, V.J., and Bécu, V., 2017. Ni-Cr metallotect: synthesis, updates, and revised models for the

Superior Province; *in* Targeted Geoscience Initiative–2016 Report of Activities, (ed.) N. Rogers; Geological Survey of Canada, Open File 8199, p. 59–61.

Houlé, M.G., Lesher, C.M., Metsaranta, R.T., and Sappin, A.-A., 2019. Architecture of magmatic conduits in chromium-PGE and Ni-Cu-PGE ore systems in Superior Province: example from the 'Ring of Fire' region, Ontario; *in* Targeted Geoscience Initiative: 2018 report of activities, (ed.) N. Rogers; Geological Survey of Canada, Open File 8549, p. 441–448.

Houlé, M.G., Lesher, C.M., Sappin, A.-A., Bédard, M.-P., Goutier, J., and Yang, X.-M., 2020. Overview of Ni-Cu-(PGE), Cr-(PGE), and Fe-Ti-V magmatic mineralization in the Superior Province: Insights on metallotects and metal Endowment; *in* Targeted Geoscience Initiative 5: Advances in the understanding of Canadian Ni-Cu-PGE and Cr ore systems—Examples from the Midcontinent Rift, the Circum-Superior Belt, the Archean Superior Province, and Cordilleran Alaskan-type intrusions, (ed.) W. Bleeker and M.G. Houlé; Geological Survey of Canada, Open File 8722, p. 117–139.

Huppert, H.E., Sparks, R.S.J., Turner, J.S., and Arndt, N.T., 1984. Emplacement and cooling of komatiite lavas; Nature, v. 309, p. 19–22.

Kavanagh, J., Boutelier, D., and Cruden, A. 2015. The mechanics of sill inception, propagation and growth: Experimental evidence for rapid reduction in magmatic overpressure; Earth and Planetary Science Letters, v. 421, p. 117–128.

Keays, R.R., 1982. Palladium and iridium in komatiites and associated rocks: Application to petrogenetic problems; *in* Komatiites, (ed.) N.T. Arndt and E.G. Nisbet; George Allen and Unwin, London, p. 435–457.

Keays, R.R. and Lightfoot, P.C., 2010. Crustal sulfur is required to form magmatic Ni–Cu sulfide deposits: evidence from chalcophile element signatures of Siberian and Deccan Trap basalts; Mineralium Deposita, v. 45, p. 241–257.

Keltie, E.E., 2018. An experimental study of the role of contamination in the formation of chromitites in the Ring of Fire intrusive suite; M.Sc. thesis, Dalhousie University, Halifax, Nova Scotia, 146 p.

Kuzmich, B. 2014. Petrogenesis of the ferrogabbroic intrusions and associated Fe-Ti-V-P mineralization within the McFaulds Lake greenstone belt, Superior Province, northern Ontario, Canada; M.Sc. thesis, Lakehead University, Thunder Bay, Ontario, 486 p.

Kuzmich, B., Hollings, P., and Houlé, M.G., 2015. Petrogenesis of the ferrogabbroic intrusions and associated Fe-Ti-V-(P) mineralization within the McFaulds greenstone belt, Superior Province, northern Ontario; *in* Targeted Geoscience Initiative 4: Canadian Nickel-Copper-Platinum Group Elements-Chromium Ore Systems—Fertility, Pathfinders, New and Revised Models, (ed.) D.E. Ames and M.G. Houlé; Geological Survey of Canada, Open File 7856, p. 115–123.

Laarman, J.E., 2014. A detailed metallogenic study of the McFaulds Lake chromite deposits, northern Ontario; Ph.D. thesis, University of Western Ontario, London, Ontario, 529 p.

Laudadio, A.B., 2019. 3D geological modelling of the Double Eagle – Black Thor intrusive complexes, McFaulds Lake greenstone belt, Ontario, Canada; M.Sc. thesis, Carleton University, Ottawa, Ontario, 107 p.

Laudadio, A.B., Schetselaar, E., and Houlé, M.G., 2018a. 3D geological modelling of the Double Eagle - Black Thor intrusive complexes, McFaulds Lake greenstone belt, Ontario, Canada; Geological Survey of Canada, Scientific Presentation 82, 1 poster.

Laudadio, A.B., Schetselaar, E., Houlé, M.G, and Samson, C., 2018b. 3D geological modelling of the Double Eagle – Black Thor intrusive complexes, McFaulds Lake greenstone belt, Ontario; *in* Targeted Geoscience Initiative: 2017 report of activities, volume 2, (ed.) N. Rogers; Geological Survey of Canada, Open File 8373, p. 35–41.

Lesher, C.M., 1989. Komatiite-associated nickel sulfide deposits; *in* Ore Deposition Associated with Magmas, (ed.) J.A. Whitney and A.J. Naldrett; Reviews in Economic Geology, v. 4, p. 45–101.

Lesher, C.M., 2007. Ni-Cu-(PGE) deposits in the Raglan area, Cape Smith Belt, New Québec; *in* Mineral Deposits of Canada: A Synthesis of Major Deposit-Types, District Metallogeny, the Evolution of Geological Provinces, and Exploration Methods, (ed.) W.D. Goodfellow; Geological Association of Canada, Mineral Deposits Division, Special Publication no. 5, p. 351–386.

Lesher, C.M., 2017. Roles of residues/skarns, xenoliths, xenocrysts, xenomelts, and xenovolatiles in the genesis, transport, and localization of magmatic Fe-Ni-Cu-PGE sulfides and chromite; Ore Geology Reviews, v. 90, p. 465-484.

Lesher, C.M., 2019. Up, down, or sideways: Emplacement of magmatic Ni-Cu±PGE sulfide melts in Large Igneous Provinces; Canadian Journal Earth Sciences, v. 56, p. 756–773.

Lesher, C.M. and Barnes, S.J., 2009. Komatiite-associated Ni-Cu-(PGE) deposits; *in* Magmatic Ni-Cu-PGE Deposits: Genetic Models and Exploration, (ed.) C. Li and E.M. Ripley; Geological Publishing House of China, p. 27–101.

Lesher, C.M. and Campbell, I.H., 1993. Geochemical and fluid dynamic modeling of compositional variations in Archean komatiite-hosted nickel sulfide ores in Western Australia; Economic Geology, v. 88, p. 804–816.

Lesher, C.M. and Groves, D.I., 1986. Controls on the formation of komatiite associated nickel–copper sulfide deposits; *in* Geology and Metallogeny of Copper Deposits, (ed.) G.H. Friedrich, A. Genkin, A.J. Naldrett, J.D. Ridge, R.H. Sillitoe, and F.M. Vokes; Proceedings of the Twenty-Seventh International Geological Congress, Moscow, Springer, Germany, p. 43–62.

Lesher, C.M. and Keays, R.R., 2002. Komatiite-associated Ni-Cu-(PGE) deposits: Mineralogy, geochemistry, and genesis; *in* The Geology, Geochemistry, Mineralogy, and Mineral Beneficiation of the Platinum-Group Elements, (ed.) L.J. Cabri; Canadian Institute of Mining, Metallurgy, and Petroleum, Special volume 54, p. 579–617.

Lesher, C.M. and Stone, W.E., 1996. Exploration geochemistry of komatiites; *in* Igneous Trace Element Geochemistry: Applications for Massive Sulphide Exploration, (ed.) D. Wyman; Geological Association of Canada, Short Course Notes 12, p. 153–204.

Lesher, C.M., Arndt, N.T., and Groves, D.I., 1984. Genesis of komatiite-associated nickel sulphide deposits at Kambalda, Western Australia: a distal volcanic model; *in* Sulphide Deposits in Mafic and Ultramafic Rocks, (ed.) D.L. Buchanan and M.J. Jones; Institute of Mining and Metallurgy, United Kingdom, p. 70–80.

Lesher, C.M., Burnham, O.M., Keays, R.R., Barnes, S.J., and Hulbert, L., 2001. Geochemical discrimination of barren and mineralized komatiites associated with magmatic Ni-Cu-(PGE) sulphide deposits; The Canadian Mineralogist, v. 39, p. 673–696.

Lesher, C.M., Carson, H.J.E, and Houlé, M.G., 2019. Genesis of chromite deposits by dynamic upgrading of Fe±Ti oxide xenocrysts; Geology, v. 47, p. 207–210.

Lu, Y., Lesher, C.M., and Deng, J., 2019. Geochemistry and genesis of magmatic Ni-Cu±PGE and PGE deposits in China; Ore Geology Reviews, v. 107, p. 863–887.

Magee, C., Muirhead, J.D., Karvelas, A., Holford, S.P., Jack-son, C.A.L., Bastow, I.D., Schofield, N.J., Stevenson, C.T.E.,

McLean, C., McCarthy, W., and Shtukert, O., 2016. Lateral magma flow in mafic sill complexes; Geosphere, v. 12, p. 809–841.

Metsaranta, R.T., 2017. Lithogeochemical data, magnetic susceptibility data and outcrop photographs from the Winiskisis Channel, McFaulds Lake and Highbank Lake areas, "Ring of Fire" region, northern Ontario; Ontario Geological Survey, Miscellaneous Release—Data 347.

Metsaranta, R.T. and Houlé, M.G., 2017a. Precambrian geology Winiskisis Channel area, "Ring of Fire Region", north sheet; Ontario Geological Survey, Preliminary Map P.3804; Geological Survey of Canada, Open File 8200, scale 1:100 000.

Metsaranta, R.T. and Houlé, M.G., 2017b. Precambrian geology of the McFaulds Lake area, "Ring of Fire Region" – central sheet; Ontario Geological Survey, Preliminary Map P.3805; Geological Survey of Canada, Open File 8201, scale 1:100 000.

Metsaranta, R.T. and Houlé, M.G., 2017c. Precambrian geology of the Highbank Lake area – "Ring of Fire Region", southern sheet; Ontario Geological Survey, Preliminary Map P.3806; Geological Survey of Canada, Open File 8202, scale 1:100 000.

Metsaranta, R.T. and Houlé, M.G., 2020. Precambrian geology of the McFaulds Lake "Ring of Fire" region, northern Ontario; Ontario Geological Survey, Open File Report 6359, 260 p.

Metsaranta, R.T., Houlé, M.G., McNicoll, V.J., and Kamo, S.L., 2015. Revised geological framework for the McFaulds Lake greenstone belt, Ontario; *in* Targeted Geoscience Initiative 4: Canadian Nickel-Copper-Platinum Group Elements-Chromium Ore Systems—Fertility, Pathfinders, New and Revised Models, (ed.) D.E. Ames and M.G. Houlé; Geological Survey of Canada, Open File 7856, p. 61–73.

Mungall, J.E., 2007. Crustal contamination of picritic magmas during transport through dikes: The Expo intrusive suite, Cape Smith Fold Belt, New Quebec; Journal of Petrology, v. 48, p. 1021–1039.

Mungall, J.E., Harvey, J.D., Balch, S.J., Azar, B., Atkinson, J., and Hamilton, M.A., 2010. Eagle's Nest: A magmatic Ni-sulfide deposit in the James Bay Lowlands, Ontario, Canada; *in* The Challenge of Finding New Mineral Resources: Global Metallogeny, Innovative Exploration, and New Discoveries, Volume I: Gold, Silver, and Copper-Molybdenum, (ed.) R.J. Goldfarb, E.E. Marsh, and T. Monecke; Society of Economic Geologists, Special Publication 15, p. 539–559.

Mungall, J.E., Azar, B., and Hamilton, M. 2011. Ni-Cu-PGE-Cr-Fe-Ti-V and VMS mineralisation of the Ring of Fire intrusive suite, Ontario; Geological Association of Canada–Mineralogical Association of Canada, Program with Abstracts, v. 34, p. 148.

Namur, O., Abily, B., Boudreau, A., Blanchette, F., Bush, J., Ceuleneer, G., Charlier, B., Donaldson, C., Duchesne, J.C., Higgins, M., Morata, D., Nielsen, T., O'Driscoll, B., Pang, K.-N., Peacock, T., Spandler, C., Toramaru, A., and Veksler, I., 2015. Igneous layering in basaltic magma chambers; *in* Layered Intrusions, (ed.) B. Charlier, O. Namur, R. Latypov, and C. Tegner; Springer Geology, p. 75–152.

Ontario Geological Survey–Geological Survey of Canada (OGS–GSC) 2011. Ontario airborne geophysical surveys, gravity gradiometer and magnetic data, grid and profile data (ASCII and Geosoft® formats) and vector data, McFaulds Lake area; Ontario Geological Survey, Geophysical Data Set 1068.

Perring, C.S., Barnes, S.J., and Hill, R.E.T., 1995. The physical volcanology of Archaean komatiite sequences from Forrestania, Southern Cross Province, Western Australia; Lithos, v. 34, p. 189–207.

Perring, C.S., Barnes, S.J., and Hill, R.E.T., 1996. Geochemistry of komatiites from Forrestania, Southern Cross Province, Western Australia: Evidence for crustal contamination; Lithos, v. 37, p. 181–197.

Prendergast, M.D., 2001. Komatiite-hosted Hunters Road nickel deposit, central Zimbabwe: physical volcanology and sulfide genesis; Australian Journal of Earth Science, v. 48, p.681–694.

Prendergast, M.D., 2008. Archean komatiitic sill-hosted chromite deposits in the Zimbabwe craton; Economic Geology, v. 103, p. 981–1004.

Ripley, E.M. and Li, C., 2013. Sulfide saturation in mafic magmas: Is external sulfur required for magmatic Ni-Cu-(PGE) ore genesis?; Economic Geology, v. 108, p. 45–58.

Rubin, A.M. and Pollard, D.D., 1987. Origins of blade-shaped dikes in volcanic rift zones; *in* Volcanism in Hawaii, (ed.) R.W. Decker, T.L. Wright, and P.H. Stauffer; United States Geological Survey, Professional Paper 1350, v 2, p. 1449–1470.

Sage, R.P., 2000. Kimberlites of the Attawapiskat area, James Bay lowlands, northern Ontario; Ontario Geological Survey, Open File Report 6019, 341 p.

Sakai, H., Casadevall, T.J., and Moore, J.G., 1982. Chemistry and isotope ratios of sulfur in basalts and volcanic gases at Kileuea volcano, Hawaii; Geochimica et Cosmochimica Acta, v. 46, p. 729–738.

Sakai, H., Des Marais, D.J., Ueda, A., and Moore, J.G., 1984. Concentrations and isotope ratios of carbon, nitrogen, and sulfur in ocean-floor basalts; Geochimica et Cosmochimica Acta, v. 48, p. 2433–2441.

Sappin, A.-A., Houlé, M.G., Lesher, C.M., Metsaranta, R.T., and McNicoll, V.J., 2015. Regional characterization of mafic-ultramafic intrusions in the Oxford-Stull and Uchi domains, Superior Province, Ontario; *in* Targeted Geoscience Initiative 4: Canadian Nickel-Copper-Platinum Group Elements-Chromium Ore Systems—Fertility, Pathfinders, New and Revised Models, (ed.) D.E. Ames and M.G. Houlé; Geological Survey of Canada, Open File 7856, p. 75–85.

Shelley D., 1988. Radial dikes of Lyttleton Volcano—their structure, form, and petrography; New Zealand Journal of Geology and Geophysics, v. 31, p. 65–75.

Spath, C.S., III, 2017. Geology and genesis of hybridized ultramafic rocks in the Black Label hybrid zone of the Black Thor intrusive complex, McFaulds Lake greenstone belt, Ontario, Canada; M.Sc. thesis, Laurentian University, Sudbury, Ontario, 94 p.

Stott, G.M. and Josey, S.D., 2009. Post-Archean mafic (diabase) dikes and other intrusions of northwestern Ontario, north of latitude 49°30′; Ontario Geological Survey, Miscellaneous Release—Data 241.

Townsend, M.R, Pollard, D.D., and Smith, R.P., 2017. Mechanical models for dikes: A third school of thought; Tectonophysics, v. 703-704, p. 98–118.

Tuchscherer, M.G., Hoy, D., Johnson, M., Shinkle, D., Kruze, R., and Holmes, M., 2010. Fall 2008 to winter 2009 Technical drill report on the Black Thor chromite deposit, Black Label chromite zone, and associated Ni-Cu-PGEs, McFaulds property (100%), James Bay Lowlands, northern Ontario, Latitude 52º78′ N, longitude -86º20′ W; Freewest Resources Canada Ltd., unpublished report, 62 p.

Zuccarelli, N., in prep. Sulfide textural variations and multiphase ore emplacement in the Eagle's Nest Ni-Cu-(PGE) deposit, McFaulds Lake greenstone belt, Superior Province, Ontario, Canada; M.Sc. thesis, Laurentian University, Sudbury, Ontario.

Zuccarelli, N., Lesher, C.M., Houlé, M.G., and Weston, R.J., 2017. Sulfide textural variations and multiphase ore emplacement in the Eagle's Nest Ni-Cu-PGE deposit, McFaulds Lake greenstone belt, Ontario, Canada; Society for Geology Applied to Mineral Deposits, Proceeding of the 14th SGA Biennial

Meeting, p. 583–586.

Zuccarelli, N., Lesher, C.M., Houlé, M.G., and Weston, R.J., 2018a. Sulfide textural variations and multiphase ore emplacement in the Eagle's Nest Ni-Cu-(PGE) deposit, McFaulds Lake greenstone belt, Superior Province, northern Ontario, Canada; Geological Society of America, Abstracts with Programs, v. 50. doi:10.1130/abs/2018AM-317024

Zuccarelli, N., Lesher, C.M., and Houlé, M.G., 2018b. Sulphide textural variations and multiphase ore emplacement in the Eagle's Nest Ni-Cu-(PGE) deposit, McFaulds Lake greenstone belt, Ontario; *in* Targeted Geoscience Initiative: 2017 report of activities, volume 2, (ed.) N. Rogers; Geological Survey of Canada, Open File 8373, p. 29–34.

Zuccarelli, N., Lesher, C.M., Houlé, M.G., and Barnes, S.J., 2020. Variations in the textural facies of sulphide minerals in the Eagle's Nest Ni-Cu-(PGE) deposit, McFaulds Lake greenstone belt, Superior Province, Ontario: Insights from microbeam scanning energy-dispersive X-ray fluorescence spectrometry; *in* Targeted Geoscience Initiative 5: Advances in the understanding of Canadian Ni-Cu-PGE and Cr ore systems—Examples from the Midcontinent Rift, the Circum-Superior Belt, the Archean Superior Province, and Cordilleran Alaskan-type intrusions, (ed.) W. Bleeker and M.G. Houlé; Geological Survey of Canada, Open File 8722, p. 165–179.